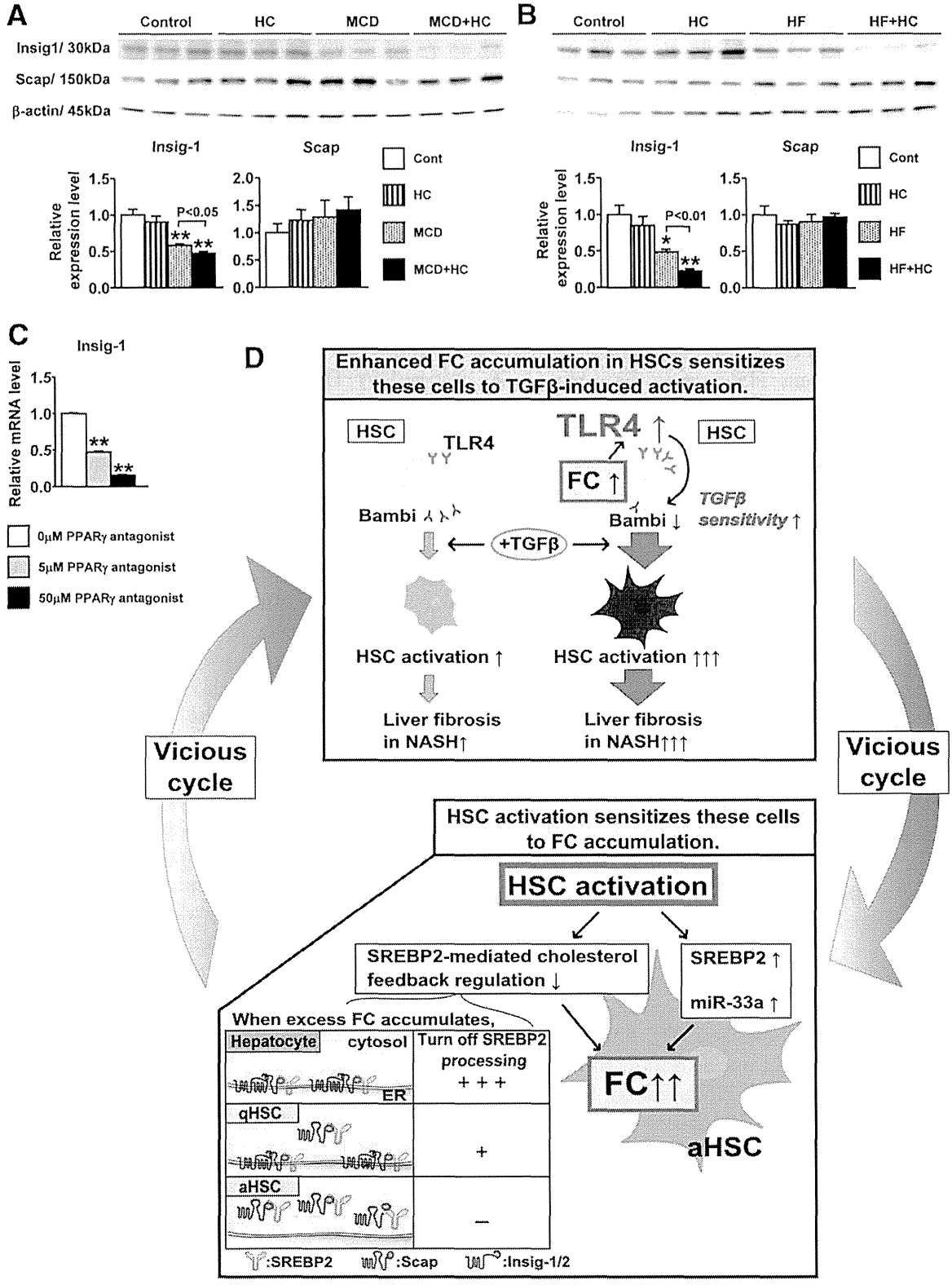

Fig. 8. Down-regulation of Insig-1 expression by HSC activation through the suppression of PPARγ signal transduction. C57BL/6 mice (9 weeks old, male; n = 6-9/group) were fed (A) the control, HC, MCD, or MCD+HC diet for 12 weeks or (B) the control, HC, HF, or HF+HC diet for 24 weeks. (A,B) Expression and quantification of Insig-1 and Scap protein in HSCs isolated from the mice in each group. $^{**}P < 0.01$ and $^{*}P < 0.05$, compared with the control diet group. (C) Quantification of Insig-1 mRNA in quiescent HSCs treated with the PPARγ antagonist. $^{**}P < 0.01$, compared with the control culture. All data are expressed as means (SEM). (D) Schematic of the characteristic mechanisms of FC accumulation in HSCs during the development of liver fibrosis in NASH. FC loading of HSCs is not sufficient to induce activation but serves to enhance activation initiated by TGFβ. Enhanced FC accumulation in HSCs plays an important role in the progression of liver fibrosis in NASH by promoting TLR4 signal transduction through suppression of the endosomal-lysosomal degradation pathway of TLR4, down-regulating the Bambi expression level, and subsequently sensitizing HSCs to TGFβ-induced activation. HSCs are sensitive to FC accumulation because of the high intracellular Scap-to-Insig expression ratio, and furthermore, HSC activation dysregulates their cholesterol metabolism, resulting in further FC accumulation and exaggerating liver fibrosis in a vicious cycle.

cholesterol and/or activation of HSCs. They also suggest that such accumulation could play an important role as a mediator of the vicious cycle of HSC activation in NASH (Fig. 8D).

There are two major pathways for cell surface receptor degradation after ubiquitination: a ubiquitin-proteasome pathway and a lysosomal degradation pathway.[16] Our present results showed that FC accumulation in HSCs inhibited the degradation of TLR4, mainly by down-regulating a lysosomal degradation pathway, which resulted in increased levels of TLR4 protein. These results are compatible with our previous report[3] showing that FC accumulation in HSCs could be involved in endosomal-lysosomal dysfunction.

The MCD diet-induced mouse model is commonly used as a model of NASH, and the resulting characteristic pathology of steatosis, mixed cell inflammatory infiltrate, hepatocellular necrosis, and pericellular fibrosis mimics that found in humans with NASH.[17,18] Nevertheless, the mice do not develop the accompanying metabolic syndrome that is often associated with human NASH. Therefore, we also used an HF diet-induced model of NASH to examine the precise role of cholesterol in the pathophysiology of NASH. As the results were similar in both mouse models of NASH, our findings may indicate a role for cholesterol in the pathophysiology of NASH.

Mari et al.[19] reported that mitochondrial FC loading accounted for hepatocellular sensitivity to TNFα. Furthermore, they showed that the mitochondrial FC content in mouse hepatocytes increased transiently only during the first 6 days of HC feeding, and thereafter returned to its prior level.[19] Our results also showed that chronic HC feeding did not significantly increase mitochondrial FC accumulation in hepatocytes. This could be one reason why an increased intake of cholesterol did not impact the hepatocellular damage in our two mouse models of NASH.

A recent report showed that accumulation of cholesterol in the lysosomes of Kupffer cells increased hepatic inflammation in the mouse model of NAFLD.[20] 27-Hydroxycholesterol is enzymatically generated from mitochondrial cholesterol by the mitochondrial P450 enzyme, Cyp27a1.[21] Further, it mobilizes cholesterol from the lysosomes to the cytoplasm, resulting in a reduction in the accumulation of lysosomal cholesterol in Kupffer cells.[20] In both mouse models of NASH, an increased intake of cholesterol did not affect the lysosomal cholesterol levels in Kupffer cells, nor did it impact the mitochondrial cholesterol levels or Cyp27a1 expression levels in Kupffer cells. These could be some reasons why increased cholesterol intake did not accelerate Kupffer cell activation in our mouse models of NASH.

In conclusion, FC accumulation in HSCs was enhanced mainly by two mechanisms: enhancement of both SREBP2 and miR-33a signaling through the suppression of PPARγ signaling along with HSC activation and disruption of the SREBP2-mediated cholesterol-feedback system in HSCs, which was characterized by a high Scap-to-Insig ratio and exaggerated by the down-regulation of Insig-1 through the suppression of PPARγ signaling along with HSC activation. Enhanced FC accumulation in HSCs plays an important role in the progression of liver fibrosis in NASH by promoting TLR4 signal transduction through suppression of the endosomal-lysosomal degradation pathway of TLR4, and subsequently sensitizing HSCs to TGFβ-induced activation. HSC activation dysregulates their cholesterol metabolism, resulting in further FC accumulation and exaggerating liver fibrosis in a vicious cycle (Fig. 8D). We believe that the characteristic mechanisms of FC accumulation in HSCs should be further studied as potential targets to treat liver fibrosis in liver diseases including NASH.

Acknowledgment: The authors thank Mina Kitazume and Miho Takabe (Keio University) for helpful advice and technical assistance, and Drs. Ikuo Inoue and Makoto Seo (Saitama Medical School) for helpful discussion and critical comments.

References

1. Schattenberg JM, Schuppan D. Nonalcoholic steatohepatitis: the therapeutic challenge of a global epidemic. Curr Opin Lipidol 2011;22:479-488.
2. Musso G, Cassader M, Gambino R. Cholesterol-lowering therapy for the treatment of nonalcoholic fatty liver disease: an update. Curr Opin Lipidol 2011;22:489-496.
3. Teratani T, Tomita K, Suzuki T, Oshikawa T, Yokoyama H, Shimamura K, et al. A high-cholesterol diet exacerbates liver fibrosis in mice via accumulation of free cholesterol in hepatic stellate cells. Gastroenterology 2012;142:152-164 e110.
4. Bengoechea-Alonso MT, Ericsson J. SREBP in signal transduction: cholesterol metabolism and beyond. Curr Opin Cell Biol 2007;19:215-222.
5. Radhakrishnan A, Goldstein JL, McDonald JG, Brown MS. Switch-like control of SREBP-2 transport triggered by small changes in ER cholesterol: a delicate balance. Cell Metab 2008;8:512-521.
6. Horton JD, Shah NA, Warrington JA, Anderson NN, Park SW, Brown MS, et al. Combined analysis of oligonucleotide microarray data from transgenic and knockout mice identifies direct SREBP target genes. Proc Natl Acad Sci U S A 2003;100:12027-12032.
7. Brown MS, Goldstein JL. A proteolytic pathway that controls the cholesterol content of membranes, cells, and blood. Proc Natl Acad Sci U S A 1999;96:11041-11048.
8. Nohturfft A, Brown MS, Goldstein JL. Sterols regulate processing of carbohydrate chains of wild-type SREBP cleavage-activating protein (SCAP), but not sterol-resistant mutants Y298C or D443N. Proc Natl Acad Sci U S A 1998;95:12848-12853.

9. Radhakrishnan A, Sun LP, Kwon HJ, Brown MS, Goldstein JL. Direct binding of cholesterol to the purified membrane region of SCAP: mechanism for a sterol-sensing domain. Mol Cell 2004;15:259-268.
10. Bommer GT, MacDougald OA. Regulation of lipid homeostasis by the bifunctional SREBF2-miR33a locus. Cell Metab 2011;13:241-247.
11. Adams CM, Reitz J, De Brabander JK, Feramisco JD, Li L, Brown MS, et al. Cholesterol and 25-hydroxycholesterol inhibit activation of SREBPs by different mechanisms, both involving SCAP and Insigs. J Biol Chem 2004;279:52772-52780.
12. Abi-Mosleh L, Infante RE, Radhakrishnan A, Goldstein JL, Brown MS. Cyclodextrin overcomes deficient lysosome-to-endoplasmic reticulum transport of cholesterol in Niemann-Pick type C cells. Proc Natl Acad Sci U S A 2009;106:19316-19321.
13. Brown AJ, Sun L, Feramisco JD, Brown MS, Goldstein JL. Cholesterol addition to ER membranes alters conformation of SCAP, the SREBP escort protein that regulates cholesterol metabolism. Mol Cell 2002;10: 237-245.
14. Seki E, De Minicis S, Osterreicher CH, Kluwe J, Osawa Y, Brenner DA, et al. TLR4 enhances TGF-beta signaling and hepatic fibrosis. Nat Med 2007;13:1324-1332.
15. Tsukamoto H, Zhu NL, Asahina K, Mann DA, Mann J. Epigenetic cell fate regulation of hepatic stellate cells. Hepatol Res 2011;41:675-682.
16. Chuang TH, Ulevitch RJ. Triad3A, an E3 ubiquitin-protein ligase regulating Toll-like receptors. Nat Immunol 2004;5:495-502.
17. Tomita K, Tamiya G, Ando S, Ohsumi K, Chiyo T, Mizutani A, et al. Tumour necrosis factor alpha signalling through activation of Kupffer cells plays an essential role in liver fibrosis of non-alcoholic steatohepatitis in mice. Gut 2006;55:415-424.
18. Leclercq IA, Farrell GC, Field J, Bell DR, Gonzalez FJ, Robertson GR. CYP2E1 and CYP4A as microsomal catalysts of lipid peroxides in murine nonalcoholic steatohepatitis. J Clin Invest 2000;105:1067-1075.
19. Mari M, Caballero F, Colell A, Morales A, Caballeria J, Fernandez A, et al. Mitochondrial free cholesterol loading sensitizes to TNF- and Fas-mediated steatohepatitis. Cell Metab 2006;4:185-198.
20. Bieghs V, Hendrikx T, van Gorp PJ, Verheyen F, Guichot YD, Walenbergh SM, et al. The cholesterol derivative 27-hydroxycholesterol reduces steatohepatitis in mice. Gastroenterology 2013;144:167-178 e161.
21. Umetani M, Shaul PW. 27-Hydroxycholesterol: the first identified endogenous SERM. Trends Endocrinol Metab 2011;22:130-135.

Research Article

JOURNAL OF HEPATOLOGY

Acyl-CoA:cholesterol acyltransferase 1 mediates liver fibrosis by regulating free cholesterol accumulation in hepatic stellate cells

Kengo Tomita[1,2,*,†], Toshiaki Teratani[2,†], Takahiro Suzuki[2], Motonori Shimizu[1], Hirokazu Sato[1], Kazuyuki Narimatsu[1], Shingo Usui[1], Hirotaka Furuhashi[1], Akifumi Kimura[3], Kiyoshi Nishiyama[3], Tadashi Maejima[3], Yoshikiyo Okada[1], Chie Kurihara[1], Katsuyoshi Shimamura[2], Hirotoshi Ebinuma[2], Hidetsugu Saito[4], Hirokazu Yokoyama[5], Chikako Watanabe[1], Shunsuke Komoto[1], Shigeaki Nagao[1], Kazuo Sugiyama[2], Suefumi Aosasa[3], Kazuo Hatsuse[3], Junji Yamamoto[3], Toshifumi Hibi[2], Soichiro Miura[1], Ryota Hokari[1], Takanori Kanai[2]

[1]*Division of Gastroenterology and Hepatology, Department of Internal Medicine, National Defense Medical College, 3-2 Namiki, Tokorozawa-shi, Saitama 359-8513, Japan;* [2]*Division of Gastroenterology and Hepatology, Department of Internal Medicine, Keio University School of Medicine, 35 Shinanomachi, Shinjuku-ku, Tokyo 160-8582, Japan;* [3]*Department of Surgery, National Defense Medical College, 3-2 Namiki, Tokorozawa-shi, Saitama 359-8513, Japan;* [4]*Graduate School of Pharmaceutical Sciences, Keio University Faculty of Pharmacy, 1-5-30 Shibakoen, Minato-ku, Tokyo 105-8512, Japan;* [5]*Health Center, Keio University School of Medicine, 35 Shinanomachi, Shinjuku-ku, Tokyo 160-8582, Japan*

Background & Aims: Acyl-coenzyme A: cholesterol acyltransferase (ACAT) catalyzes the conversion of free cholesterol (FC) to cholesterol ester, which prevents excess accumulation of FC. We recently found that FC accumulation in hepatic stellate cells (HSCs) plays a role in progression of liver fibrosis, but the effect of ACAT1 on liver fibrosis has not been clarified. In this study, we aimed to define the role of ACAT1 in the pathogenesis of liver fibrosis.

Methods: ACAT1-deficient and wild-type mice, or Toll-like receptor 4 ($TLR4)^{-/-}ACAT1^{+/+}$ and $TLR4^{-/-}ACAT1^{-/-}$ mice were subjected to bile duct ligation (BDL) for 3 weeks or were given carbon tetrachloride (CCl_4) for 4 weeks to induce liver fibrosis.

Results: ACAT1 was the major isozyme in mice and human primary HSCs, and ACAT2 was the major isozyme in mouse primary hepatocytes and Kupffer cells. ACAT1 deficiency significantly exaggerated liver fibrosis in the mouse models of liver fibrosis, without affecting the degree of hepatocellular injury or liver inflammation, including hepatocyte apoptosis or Kupffer cell activation. ACAT1 deficiency significantly increased FC levels in HSCs, augmenting TLR4 protein and downregulating expression of transforming growth factor-β (TGFβ) pseudoreceptor Bambi (bone morphogenetic protein and activin membrane-bound inhibitor), leading to sensitization of HSCs to TGFβ activation. Exacerbation of liver fibrosis by ACAT1 deficiency was dependent on FC accumulation-induced enhancement of TLR4 signaling.

Conclusions: ACAT1 deficiency exaggerates liver fibrosis mainly through enhanced FC accumulation in HSCs. Regulation of ACAT1 activities in HSCs could be a target for treatment of liver fibrosis.

Keywords: Acyl-coenzyme A:cholesterol acyltransferase; Free cholesterol; Hepatic stellate cell; Toll-like receptor 4; Bone morphogenetic protein and activin membrane-bound inhibitor; Transforming growth factor-β.

Received 22 October 2013; received in revised form 22 February 2014; accepted 10 March 2014; available online 18 March 2014

* Corresponding author. Address: Division of Gastroenterology and Hepatology, Department of Internal Medicine, National Defense Medical College, 3-2 Namiki, Tokorozawa-shi, Saitama 359-8513, Japan. Tel.: +81 4 2995 1211x2369; fax: +81 4 2996 5201.

E-mail address: kengo@ndmc.ac.jp (K. Tomita).

† These authors contributed equally to this work.

Abbreviations: HSC, hepatic stellate cell; FC, free cholesterol; TLR4, Toll-like receptor 4; Bambi, bone morphogenetic protein and activin membrane-bound inhibitor; TGF, transforming growth factor; CE, cholesterol ester; ACAT, acyl-coenzyme A:cholesterol acyltransferase; MβCD, methyl-β-cyclodextrin; LPS, lipopolysaccharide; CCl_4, carbon tetrachloride; BDL, bile duct ligation; ALT, alanine aminotransferase; HE, hematoxylin-eosin; SMA, smooth muscle actin; TUNEL, terminal deoxynucleotidyl transferase-mediated deoxyuridine nick-end labeling; PCR, polymerase chain reaction; TNF, tumor necrosis factor; VCAM-1, vascular cell adhesion molecule-1; ICAM-1, intercellular adhesion molecule-1; MCP-1, monocyte chemoattractant protein-1.

Introduction

Although advanced liver fibrosis results in cirrhosis, liver failure, hepatocellular carcinoma, and portal hypertension and often requires liver transplantation, there is no standard treatment [1]. Hepatic stellate cells (HSCs) are the primary effectors, orchestrating the deposition of extracellular matrix in normal and fibrotic liver, and play a key role in the progression of liver fibrosis [2].

We recently reported that accumulation of free cholesterol (FC) in HSCs promoted Toll-like receptor 4 (TLR4) signal transduction by increasing membrane TLR4 levels, thereby downregulating bone morphogenetic protein and activin membrane-bound inhibitor (Bambi), and consequently sensitizing HSCs to transforming growth factor (TGF) β, resulting in HSC activation and progression of liver fibrosis [3]. These results suggest that the mechanism of FC metabolism in HSCs could play a pivotal role in HSC activation and liver fibrosis.

Excess cellular cholesterol is stored as cholesteryl esters (CE). The conversion of FC to CE is catalyzed by acyl-coenzyme A (CoA):cholesterol acyltransferase (ACAT) [4]. In mammals, isoenzymes ACAT1 and ACAT2, encoded by 2 different genes, mediate cellular cholesterol homeostasis, dietary cholesterol absorption, and lipoprotein assembly [4].

Mammalian ACAT1 is expressed in many different tissues and cell types; ACAT2 is expressed mainly in the liver and intestine. In mice, ACAT2 plays a key role in providing CE to chylomicrons in the intestine and mediates storage and packaging of CE into apoB-containing lipoproteins in the liver [4]. Our study showed that ACAT2 is the major isoenzyme of hepatocytes and Kupffer cells and ACAT1 is the major isoenzyme of HSCs in the mouse liver. We also demonstrated that ACAT1 is the major isoenzyme of human HSCs. These results suggest ACAT1 could play a key role in FC accumulation in HSCs.

We hypothesized that regulation of ACAT1 could play a role in the pathogenesis of liver fibrosis. We used ACAT1-deficient mice and wild-type mice in the two mouse models of liver fibrosis.

Materials and methods

Isolation of human HSCs

Human HSCs were isolated from fragments of normal livers (N = 3) obtained during surgery for colorectal liver metastasis, as described previously [5]. Briefly, after a combined digestion of liver tissue with collagenase and pronase, HSCs were separated from other non-parenchymal cells by centrifugation over a gradient of Nycodenz (9% wt/vol; Sigma). Written informed consent was obtained from all patients. The study protocol was approved by the Ethical Committee of National Defense Medical College Hospital, and followed the ethical guidelines of the Declaration of Helsinki.

Animal model

Male 9-week-old wild-type C57BL/6 mice were purchased from CLEA Japan. *ACAT1*$^{+/-}$ mice were purchased from Jackson Laboratories (Bar Harbor, Maine, USA). *ACAT1*$^{+/+}$ (wild-type) and *ACAT1*$^{-/-}$ (*ACAT1*-deficient) littermates were obtained from crosses of *ACAT1*(+/−) mice with C57BL/6 background. C57BL/6 *TLR4*$^{-/-}$ mice were purchased from Oriental BioService (Kyoto, Japan). *TLR4*$^{-/-}$*ACAT1*$^{+/+}$ and *TLR4*$^{-/-}$*ACAT1*$^{-/-}$ littermates were obtained from crosses of *ACAT1*$^{-/-}$ mice with TLR4$^{-/-}$ mice. In the liver fibrosis experiments, 9-week-old male wild-type and ACAT1-deficient mice, or *TLR4*$^{-/-}$*ACAT1*$^{+/+}$ and *TLR4*$^{-/-}$*ACAT1*$^{-/-}$ mice were given carbon tetrachloride (CCl_4) at 5 μl (10% CCl_4 in corn oil)/g body weight, by intraperitoneal injection twice a week for 4 weeks. For bile duct ligation (BDL), anesthetized mice received midline laparotomy and the common bile duct was ligated twice with silk sutures before abdominal closure. We performed the sham operation similarly, except the bile duct was not ligated. Mice were sacrificed 3 weeks after BDL.

All animals received humane care in compliance with the National Research Council's criteria outlined in the "Guide for the Care and Use of Laboratory Animals," prepared by the US National Academy of Sciences and published by the US National Institutes of Health (Bethesda, MD).

Kupffer cell depletion

Dichloromethylene diphosphonic acid (DMDP, Clodronate)-loaded or PBS-loaded liposomes (Encapsula NanoSciences) were intravenously injected (200 μl per mouse).

Biochemical and histological analysis

Serum concentrations of alanine aminotransferase (ALT) and cholesterol were determined as described [3]. Liver cholesterol levels or the cholesterol content of HSCs were measured using the Cholesterol/Cholesteryl Ester Quantitation Kit (BioVision, Mountain View, CA), following the manufacturer's instructions. Liver tissues were fixed in 4% paraformaldehyde, embedded in paraffin, and stained with hematoxylin-eosin (HE). Liver fibrosis was assessed with Sirius red staining. For protein or RNA analysis, tissues were frozen in liquid nitrogen and stored at −80 °C.

Isolation and culture of mice HSCs

Mouse HSCs were isolated as described [6]. In some experiments, they were cultured for 6 h in DMEM containing 1% or 10% FBS in uncoated plastic tissue culture dishes, and then treated with TGFβ, MβCD, or LPS.

Hepatocyte and Kupffer cell isolation

Hepatocytes and Kupffer cells were isolated from mice as previously described [3,7].

Western blotting

Preparation of whole-cell protein extracts from HSCs, Kupffer cells, and hepatocytes, electrophoresis of whole-cell protein extracts (5 μg), and blotting were performed using antibodies against TLR4, ACAT1 (Abcam, Cambridge, UK), ACAT2 (Santa Cruz Biotechnology, CA, USA), and β-actin (Sigma), as described [3]. Cells were lysed with Complete Lysis-M (Roche Applied Science, Mannheim, Germany).

ACAT activity assay

ACAT activity assay was performed as described [8], using hepatocytes, Kupffer cells, and HSCs immediately isolated from wild-type and ACAT1-deficient mice. The ACAT activity was expressed as pmoles of cholesteryl oleate synthesized per mg cell protein per minute.

Statistical analysis

All data are expressed as the means ± standard errors of the means (s.e.m.). Statistical analyses were performed using the unpaired Student's *t* test or one-way ANOVA ($p < 0.05$ was considered significant).

Results

ACAT1 is the major isoenzyme in human and mouse HSCs

Western blotting showed that ACAT1 was the major isozyme in mouse primary HSCs (Fig. 1A). We detected little ACAT2 expression in these cells. ACAT1 was also the major isozyme in human primary HSCs freshly isolated from normal livers obtained during surgery for colorectal liver metastasis (Fig. 1B). It was also the major isozyme in human HSC cell lines such as LX2 [9] and hTERT-introduced HSCs [10] (Fig. 1B). There was little ACAT2 expression in these cells. In contrast, ACAT2 was the major isozyme in mouse primary hepatocytes and Kupffer cells (Fig. 1A). ACAT1 deficiency did not affect hepatic ACAT2 expression (Supplementary Fig. 1A). We detected very little ACAT activity in ACAT1-deficient HSCs, whereas in ACAT1-deficient Kupffer cells or hepatocytes, substantial ACAT activity remained (Fig. 1C).

ACAT1 deficiency significantly exaggerated liver fibrosis

ACAT1-deficient mice did not spontaneously progress to liver fibrosis (Fig. 1D). Next, to assess the effect of ACAT1 on liver fibrosis, ACAT1-deficient or wild-type mice underwent BDL or sham treatment for 3 weeks (Fig. 1D–F). ACAT1 deficiency significantly exaggerated liver fibrosis, as shown by Sirius red staining in liver tissue (Fig. 1D). Consistent with this, hepatic αSMA

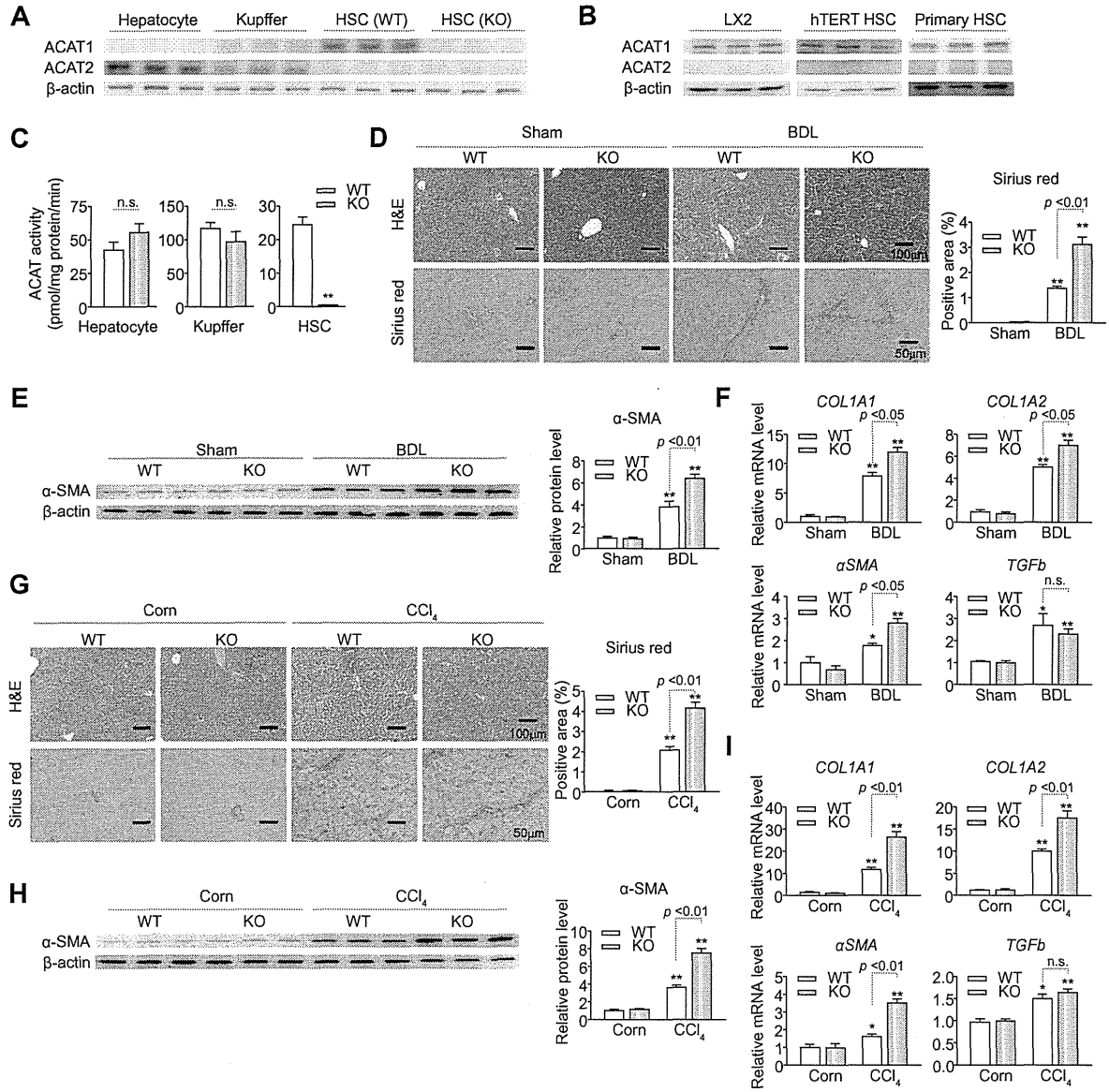

Fig. 1. Effects of ACAT1 deficiency on liver fibrosis induced by BDL or CCl_4 treatment. (A) Protein expression of ACAT1 and ACAT2 in primary cultured hepatocytes, Kupffer cells, and HSCs immediately isolated from wild-type and ACAT1-deficient mice. (B) Protein expression of ACAT1 and ACAT2 in human primary HSCs freshly isolated from normal livers (N = 3) obtained during surgery for colorectal liver metastasis and human HSC cell lines, LX-2, and hTERT-introduced HSCs. (C) ACAT activity in primary cultured hepatocytes, Kupffer cells, and HSCs isolated from wild-type and ACAT1-deficient mice (N = 4). 9-week-old male wild-type or ACAT1-deficient mice were subjected to 3-week BDL (D–F) or CCl_4 treatment twice a week for 4 weeks (G–I) to induce liver fibrosis (N = 6–8/group). (D, G) H&E-stained sections and Sirius red-stained sections in representative liver samples and quantification of Sirius red-staining. (E, H) Western blotting and quantification of hepatic αSMA expression. (F, I) Hepatic expression of collagen1α1 (*COL1A1*), collagen1α2 (*COL1A2*), αSMA, and TGFβ (*TGFb*) mRNA. n.s., not significant, *p <0.05 and **p <0.01 compared with wild-type mice–sham-operated group (D–F) or wild-type mice–corn oil group (G–I). WT, wild-type mice. KO, ACAT1-deficient mice. (This figure appears in colour on the web.)

protein expression and mRNA expression of *collagen 1α1*, *collagen 1α2*, and *αSMA* were significantly higher in ACAT1-deficient mice than in wild-type mice in the BDL-induced liver fibrosis model (Fig. 1E and F). There were no significant differences in *TGFβ* mRNA levels between ACAT1-deficient and wild-type mice (Fig. 1F).

ACAT1-deficient or wild-type mice underwent 4-week treatment with CCl_4 or corn oil (Fig. 1G–I). Similar to the BDL model, ACAT1 deficiency significantly exacerbated liver fibrosis (Fig. 1G). ACAT1 deficiency also significantly increased hepatic αSMA protein expression and transcription of *collagen 1α1*, *collagen 1α2*, and *αSMA* in the CCl_4-induced liver fibrosis model

(Fig. 1H and I). There were no significant differences in *TGFβ* mRNA levels between ACAT1-deficient and wild-type mice (Fig. 1I).

ACAT1 deficiency did not affect hepatocellular damage

ACAT1 deficiency alone was not sufficient to affect serum levels of ALT and cholesterol, or hepatic levels of total cholesterol, FC, and CE (Supplementary Fig. 1). ACAT1 deficiency also did not affect serum and hepatic cholesterol levels in the mouse models of liver fibrosis (Supplementary Fig. 1B, C, F, and G). In order to evaluate hepatocellular damage, we examined serum ALT levels and TUNEL-positive hepatocytes in liver tissues. Serum ALT levels were significantly increased in the mouse models of liver fibrosis and were unaffected by ACAT1 deficiency (Supplementary Fig. 1D and H). The numbers of TUNEL-positive hepatocytes were also significantly greater in the mouse models of liver fibrosis and were similarly unaffected by ACAT1 deficiency (Supplementary Fig. 1E and I). These results suggest ACAT1 deficiency did not influence BDL- or CCl_4-induced hepatocellular damage.

The effect of ACAT1 deficiency on liver pathology was Kupffer cell-independent

Immunohistochemistry with the Kupffer cell/macrophage marker F4/80 antibody revealed increased macrophage infiltration into the liver in both mouse models of liver fibrosis; ACAT1 deficiency had no effect (Supplementary Fig. 2A, B, D, and E). Similarly, hepatic expression of tumor necrosis factor-α (TNFα), which is produced mainly by Kupffer cells in the liver [11], was significantly increased in the mouse models of liver fibrosis and was not influenced by ACAT1 deficiency (Supplementary Fig. 2C and F). Hepatic expression of vascular cell adhesion molecule-1 (VCAM-1), inter-cellular adhesion molecule-1 (ICAM-1), CD68, monocyte chemoattractant protein-1 (MCP-1), and IL-1β were also significantly increased in the models of liver fibrosis and were unaffected by ACAT1 deficiency (Supplementary Fig. 2C and F). These results show that ACAT1 deficiency did not influence BDL- or CCl_4-induced macrophage infiltration or Kupffer cell activation.

Next, in order to eliminate the influence of Kupffer cells, ACAT1-deficient or wild-type mice were depleted of Kupffer cells by treatment with liposomal clodronate, and then treated with BDL or CCl_4 intoxication (Fig. 2 and Supplementary Fig. 3). Most Kupffer cells were depleted by treatment with liposomal clodronate in these experimental mouse models (Supplementary Fig. 3A and C). Furthermore, liposomal clodronate did not affect hepatocellular injury (Supplementary Fig. 3B and D).

ACAT1 deficiency significantly exaggerated liver fibrosis in the mouse models of liver fibrosis even in the absence of Kupffer cells (Fig. 2A and E). ACAT1 deficiency also significantly increased hepatic expression of collagen 1α1, collagen 1α2, and αSMA (Fig. 2B, C, F, and G). Serum ALT levels were not influenced by ACAT1 deficiency (Fig. 2D and H). These results suggest the effect of ACAT1 on liver fibrosis was Kupffer cell-independent.

ACAT1 deficiency sensitized HSCs to TGFβ-induced activation via increasing TLR4 protein level

HSCs were analyzed immediately after isolation from wild-type or ACAT1-deficient mice. FC contents were significantly increased in ACAT1-deficient *vs.* wild-type HSCs, whereas no significant between-genotype difference was noted in the CE level (Fig. 3A). Treatment with TGFβ significantly increased expression of *collagen 1α1*, *collagen 1α2*, and *αSMA* in HSCs; ACAT1 deficiency significantly enhanced this effect (Fig. 3B). Shortly after isolation, expression of *Bambi*, the TLR4 downstream molecule [3], was significantly lower in ACAT1-deficient than in wild-type HSCs (Fig. 3A); however no significant between-genotype difference was observed in the expression of TGFβ receptor-1 and TGFβ receptor-2 (Supplementary Fig. 4A and B). TLR4 protein levels were significantly higher in ACAT1-deficient HSCs than in wild-type HSCs, but we detected no significant between-genotype differences in the mRNA expression of *TLR4* (Fig. 3A and Supplementary Fig. 4C). Kupffer cells exhibited no significant between-genotype differences in TLR4 protein levels (Supplementary Fig. 4D). Internalization of TLR4 protein is accelerated by ligand formation, and TLR4 is transported from the cell membrane to the endosome for ubiquitination and to the lysosome for degradation [12,13]. Sixty minutes after LPS treatment, TLR4 protein expression was significantly decreased in wild-type HSCs, although the level remained high in ACAT1-deficient HSCs (Supplementary Fig. 4E).

We previously demonstrated that FC accumulation in HSCs increased TLR4 protein expression by suppressing the ligand-mediated enhanced degradation of TLR4, reduced *Bambi* expression, and sensitized HSCs to TGFβ-induced activation. Our present results suggest ACAT1 deficiency could sensitize HSCs to TGFβ-induced activation via accumulation of FC.

The effect of ACAT1 deficiency was dependent on free cholesterol in HSCs

To verify that the effects of ACAT1 deficiency are dependent on FC accumulation in HSCs, we performed experiments with methyl-β-cyclodextrin (MβCD), a membrane-impermeable cholesterol-binding agent to deplete cholesterol [14]. Treatment with MβCD dramatically reduced FC and TLR4 levels in wild-type and ACAT1-deficient HSCs to the low levels in which we could not detect significant between-genotype differences (Fig. 3C).

We detected no significant between-genotype differences in the expression of *Bambi* in HSCs cultured without LPS (Fig. 3C). LPS treatment significantly inhibited *Bambi* expression in HSCs and ACAT1 deficiency significantly enhanced this effect (Fig. 3C); the effect was ameliorated by treatment with MβCD (Fig. 3C). There were no significant genotype-related differences in *Bambi* expression in LPS-treated HSCs in the presence of MβCD (Fig. 3C). LPS-pretreated HSCs showed a significant increase in *collagen 1α1* and *αSMA* expression after TGFβ stimulation and ACAT1 deficiency significantly exaggerated this effect (Fig. 3D). The TGFβ-induced increase in *collagen 1α1* and *αSMA* expression in LPS-pretreated HSCs was ameliorated by treatment with MβCD (Fig. 3D). Further, there were no significant genotype-based differences in the *collagen 1α1* and *αSMA* expression in HSCs treated with TGFβ after addition of LPS and in the presence of MβCD (Fig. 3D). These results show that the effects of ACAT1 deficiency on HSC activation were dependent on FC accumulation.

The effect of ACAT1 deficiency on exaggeration of liver fibrosis was dependent on TLR4 signaling

Furthermore, $TLR4^{-/-}ACAT1^{+/+}$ and $TLR4^{-/-}ACAT1^{-/-}$ mice underwent BDL or sham treatment for 3 weeks (Fig. 4A and B) or

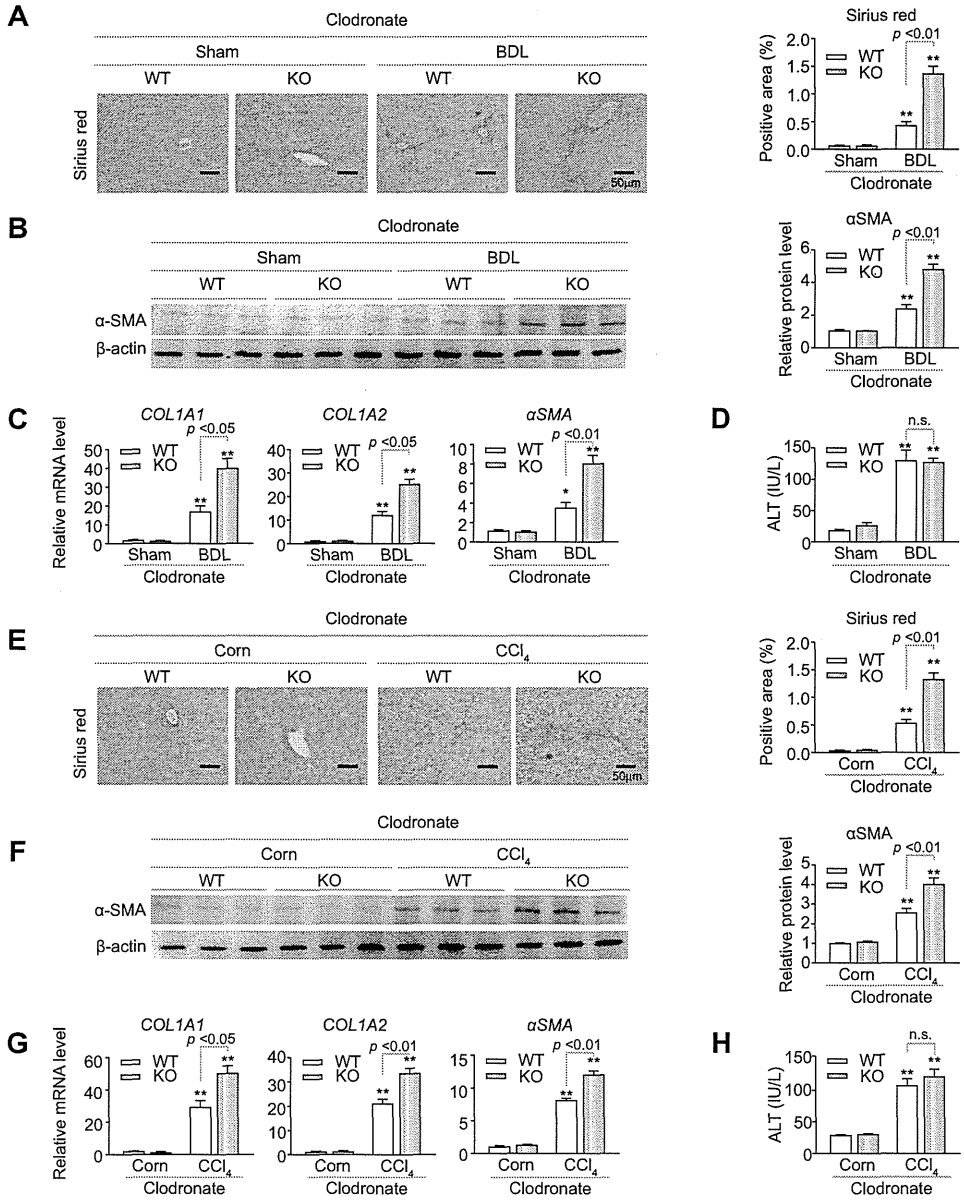

Fig. 2. Kupffer cell-independent effects of ACAT1 deficiency on hepatic fibrosis induced by BDL or CCl_4 treatment. Wild-type or ACAT1-deficient 9-week-old male mice were injected with liposomal clodronate or vehicle. Thereafter, mice were subjected to 3-week BDL (A–D) or CCl_4 treatment twice a week for 4 weeks (E–H) to induce liver fibrosis (N = 5–7/group). (A, E) Sirius red-stained sections in representative liver samples (left). Quantification of Sirius red-staining (right). (B, F) Western blotting and quantification of hepatic αSMA protein expression α. (C, G) Hepatic expression of collagen1α1 (*COL1A1*), collagen1α2 (*COL1A2*), *αSMA* mRNA. (D, H) Serum ALT levels. $^{*}p$ <0.05 and $^{**}p$ <0.01 compared with wild-type mice–sham-operated group (A–D) or wild-type mice–corn oil group (E–H). (This figure appears in colour on the web.)

4-week treatment with CCl_4 or corn oil (Fig. 4C and D) in order to assess whether the effects of ACAT1 deficiency on the mouse models of liver fibrosis were dependent on the FC accumulation-induced enhancement of TLR4 signaling. In the absence of TLR4 signaling, ACAT1 deficiency did not accelerate liver fibrosis, as shown by Sirius Red staining (Fig. 4A and C). ACAT1 deficiency also did not impact hepatic expression of collagen 1α1, collagen 1α2, and αSMA in the mouse models (Fig. 4B and D). In the absence of TLR4 signaling, FC content significantly increased in ACAT1-deficient HSCs *vs.* ACAT1-wild HSCs, whereas no significant between-genotype difference in CE was noted (Fig. 4E). Our *in vitro* analysis showed that in the absence of TLR4 signaling, ACAT1 deficiency did not affect the expression of *collagen 1α1* and *collagen 1α2* in HSCs activated by treatment with TGFβ (Fig. 4F).

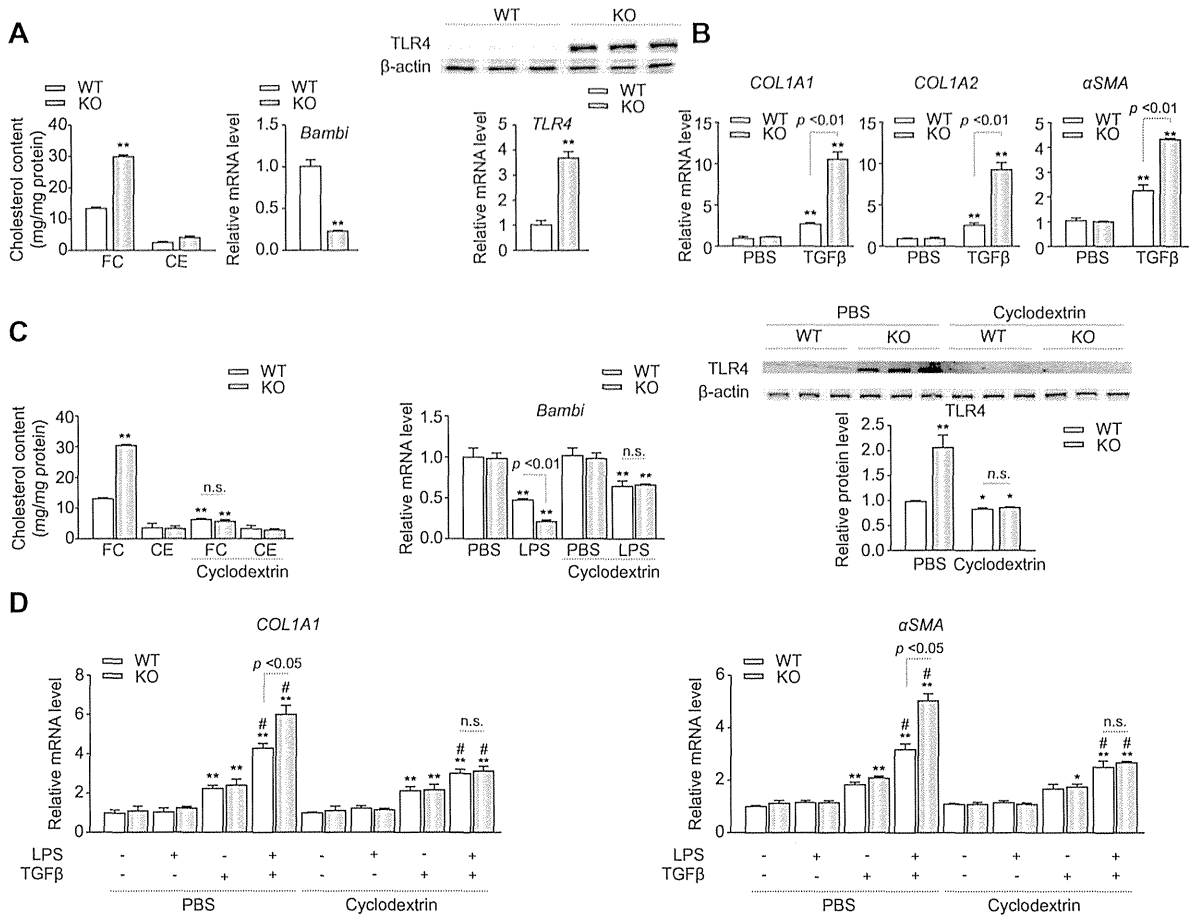

Fig. 3. Effects of ACAT1 deficiency on TGFβ-induced activation of HSC. (A) Quantification of cellular FC and CE (left panel), *Bambi* mRNA expression (middle panel), and *TLR4* protein expression (right panel) in HSCs immediately after isolation from wild-type and ACAT1-deficient mice (N = 6–7/group). $^{**}p$ <0.01 compared with wild-type HSCs. (B) Expression of collagen1α1 (*COL1A1*), collagen1α2 (*COL1A2*), *αSMA* mRNA mRNA in primary HSC cultures. Six h after isolation from wild-type or ACAT1-deficient mice, HSCs were treated with TGFβ (1 ng/ml) for 10 h (N = 6–7/group). $^{**}p$ <0.01 compared with wild-type HSCs–control culture. (C) Quantification of cellular FC and CE (left panel) and TLR4 protein (right panel) in wild-type and ACAT1-deficient HSCs. Six h after isolation, mouse HSCs were treated with MβCD for 12 h (N = 5–7/group). $^{**}p$ <0.01 compared with FC in vehicle-treated wild-type HSCs. (Middle panel) Expression of Bambi mRNA in wild-type and ACAT1-deficient HSCs. Six h after isolation, mouse HSCs were incubated with vehicle or MβCD for 12 h, followed by LPS (100 ng/ml) for 6 h (N = 5–7/group). $^{**}p$ <0.01 compared with vehicle-treated wild-type HSC cultures without LPS treatment. (D) Expression of collagen1α1 (*COL1A1*), and *αSMA* mRNA mRNA in wild-type and ACAT1-deficient HSCs. Six h after isolation, mouse HSCs were incubated with vehicle or MβCD for 12 h, followed by LPS (100 ng/ml) for 6 h, before adding TGFβ for an additional 10 h (N = 5–7/group). $^{*}p$ <0.05 and $^{**}p$ <0.01 compared with the vehicle-treated wild-type HSC control cultures. $^{\#}p$ <0.05 compared with the corresponding cultures treated with TGFβ in the absence of LPS.

Although Bambi expression was significantly lower in ACAT1-deficient HSCs than in wild-type HSCs, we detected no significant differences between *TLR4*$^{-/-}$*ACAT1*$^{+/+}$ and *TLR4*$^{-/-}$*ACAT1*$^{-/-}$ HSCs (Fig. 4G). These results suggest FC accumulation-induced TLR4 signaling could play an important role in the exacerbation of liver fibrosis by ACAT1 deficiency. TLR4-dependent genes such as *CXCL2*, *CCL7*, and *CXCL5* are positively regulated by TLR4 signaling in HSCs [15]. Shortly after isolation, expression of these genes was significantly higher in ACAT1-deficient HSCs than in wild-type HSCs; we detected no significant differences between *TLR4*$^{-/-}$*ACAT1*$^{+/+}$ and *TLR4*$^{-/-}$*ACAT1*$^{-/-}$ HSCs (Supplementary Fig. 4G). As shown in Supplementary Fig. 4E, the level of TLR4 protein expression remained high in ACAT1-deficient HSCs after LPS treatment in comparison to wild-type HSCs. Consistent with these results, the increased expression in TLR4 dependent genes after LPS treatment was significantly greater in ACAT1-deficient HSCs than in wild-type HSCs (Supplementary Fig. 4F).

Discussion

In this study, we found that ACAT1 deficiency exaggerated BDL- and CCl_4-induced liver fibrosis, without affecting hepatocyte injury or Kupffer cell activation. This could be because ACAT1 is the major ACAT isozyme in HSCs, while ACAT2 is the major

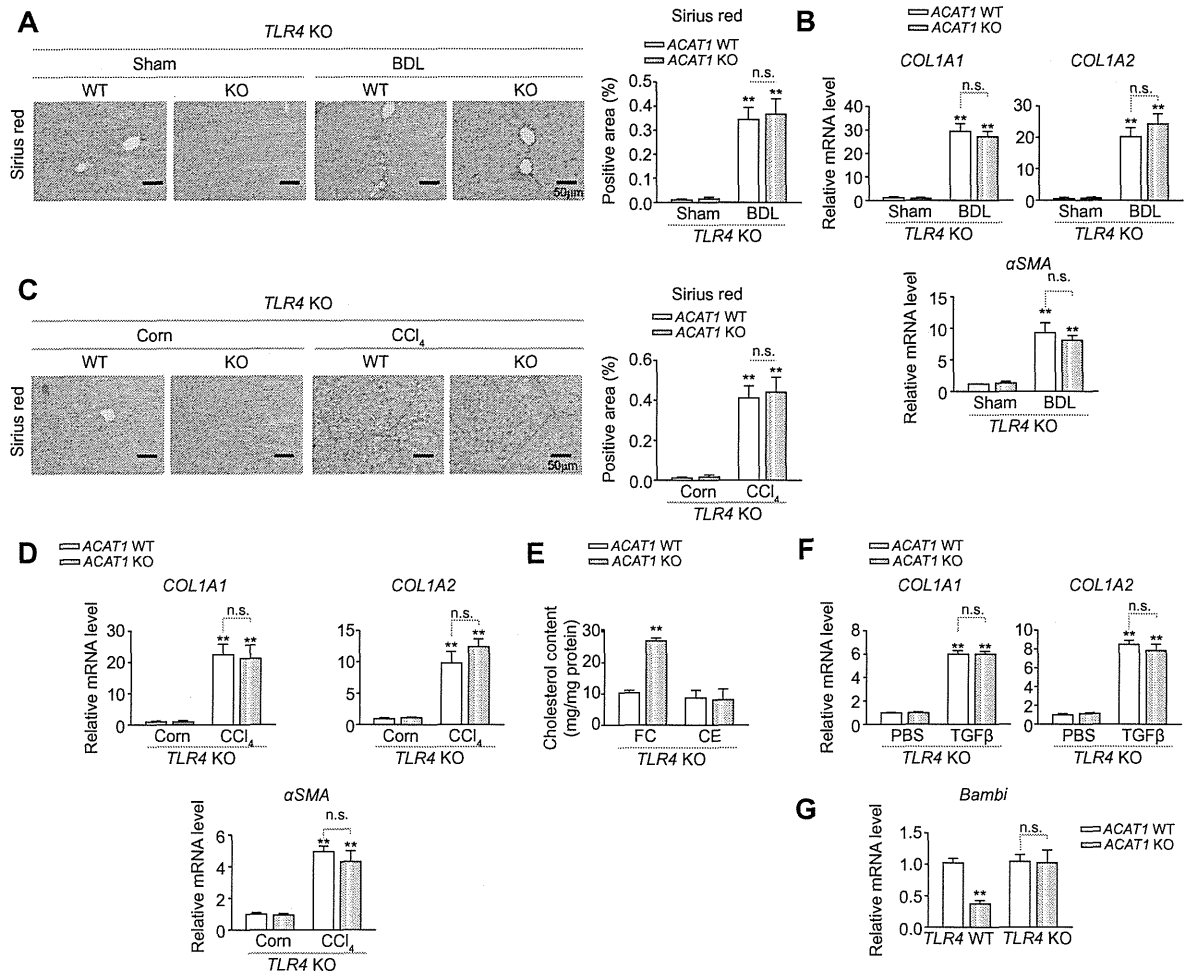

Fig. 4. Effects of ACAT1 deficiency on liver fibrosis of TLR4-deficient mice, induced by BDL or CCl_4 treatment. *TLR4*$^{-/-}$*ACAT1*$^{+/+}$ or *TLR4*$^{-/-}$*ACAT1*$^{-/-}$ mice (9-weeks old) were subjected to 3-week BDL (A, B) or CCl_4 treatment twice a week for 4 weeks (C, D) to induce liver fibrosis (N = 6–8/group). (A, C) Sirius red-stained sections in representative liver samples. Quantification of Sirius red-staining. (B, D) Hepatic expression of collagen1α1 (*COL1A1*), collagen1α2 (*COL1A2*), *αSMA* mRNA. $^{**}p$ <0.01 compared with *TLR4*$^{-/-}$*ACAT1*$^{+/+}$ mice–sham-operated group (A, B) or *TLR4*$^{-/-}$*ACAT1*$^{+/+}$ mice–corn oil group (C, D). WT, *TLR4*$^{-/-}$*ACAT1*$^{+/+}$ mice. KO, *TLR4*$^{-/-}$*ACAT1*$^{-/-}$ mice. (E) Quantification of cellular FC and CE in HSCs immediately after isolation from *TLR4*$^{-/-}$*ACAT1*$^{+/+}$ and *TLR4*$^{-/-}$*ACAT1*$^{-/-}$ mice (N = 6–7/group). $^{**}p$ <0.01 compared with *TLR4*$^{-/-}$*ACAT1*$^{+/+}$ HSCs. (F) Expression of collagen1α1 (*COL1A1*), and collagen1α2 (*COL1A2*) mRNA in primary HSC cultures. Primary HSCs isolated from *TLR4*$^{-/-}$*ACAT1*$^{+/+}$ mice or *TLR4*$^{-/-}$*ACAT1*$^{-/-}$ mice were treated with TGFβ (1 ng/ml) for 6 h (N = 5–7/group). $^{**}p$ <0.01 compared with TLR4$^{-/-}$*ACAT1*$^{+/+}$ HSCs–control culture. (G) Expression of *Bambi* mRNA in HSCs immediately after isolation from *TLR4*$^{+/+}$*ACAT1*$^{+/+}$, *TLR4*$^{+/+}$*ACAT1*$^{-/-}$, *TLR4*$^{-/-}$*ACAT1*$^{+/+}$, and *TLR4*$^{-/-}$*ACAT1*$^{-/-}$ mice (N = 5–7/group). $^{**}p$ <0.01 compared with *TLR4*$^{+/+}$*ACAT1*$^{+/+}$ HSCs. (This figure appears in colour on the web.)

isozyme in hepatocytes and Kupffer cells. FC accumulation in HSCs was significantly enhanced in ACAT1-deficient mice. As a result, ACAT1 deficiency exacerbated liver fibrosis in the two mouse models of liver fibrosis mainly via FC accumulation in HSCs, which increased TLR4 protein levels and sensitized HSCs to TGFβ by down-regulating Bambi expression.

Cells acquire cholesterol mainly from low-density lipoprotein (LDL) and *de novo* biosynthesis [4]. Cholesterol molecules from both sources move within the cells, eventually reaching the ER; a portion is converted to CE, which mainly exists as cytosolic lipid droplets, primarily by ACAT1 [4,16]. CE biosynthesis and hydrolysis occurs continuously, forming the FC/CE cycle. ACAT1 preferentially reutilizes FC released from the CEs [16]. In this study, we showed that ACAT1 is a key regulator of FC accumulation in HSCs. We also found that HSCs contain most of cholesterol in the form of FC, not CE. Thus, ACAT1 deficiency in HSCs increases FC accumulation, but does not affect CE accumulation. FC accumulation in HSCs caused by ACAT1 deficiency suppressed ligand-mediated degradation of TLR4. These results were consistent with our previous reports [3].

In atherosclerosis, chronic accumulation of CE in macrophages cause them to appear foamy and is a hallmark of early atherosclerosis [4]. Therefore, numerous ACAT inhibitors have been synthesized and tested for their utility in treating atherosclerosis, although their utility as anti-atherosclerosis drugs is unclear [4]. In patients with hypercholesterolemia, treatment with an ACAT inhibitor failed to improve atherosclerosis but was associated with carotid atherosclerosis progression and increased

incidence of major cardiovascular events [17]. Similarly, ACAT inhibition was not an effective strategy for limiting atherosclerosis; indeed, it promoted atherogenesis in patients with coronary disease [18]. Selective inhibition of ACAT1 in lesion macrophages associated with hyperlipidemia resulted in FC accumulation in the artery wall and promoted lesion development [19,20]. Other reports have shown that augmented FC accumulation in ACAT1-deficient macrophages played a central role in the development of atherosclerosis [21,22]. The accumulation of excess intracellular FC is cytotoxic [23]. As a cytotoxic component, FC accumulation in the ER membrane enhances ER stress, resulting in cellular apoptosis in macrophages *in vitro* and *in vivo* [24,25]. Further, recent reports have shown that the age-related increase in intrathymic FC accumulation causes NLRP3 inflammasome activation as a lipotoxic danger signal and participates in age-related thymic involution [26]. These results suggest the major effect of reduced ACAT1 activities on the pathophysiology of human diseases could be due to increased cellular FC accumulation, not decreased cellular CE accumulation.

As membrane organization is important for many basic cell functions, changes in FC by ACAT1 could have a role in many diseases [23]. FC accumulation in HSCs played a major role in the pathogenesis of liver fibrosis; therefore, regulation of ACAT1 in HSCs could be a new treatment strategy for liver fibrosis. Some reports in human subjects showed that ACAT1 gene polymorphisms affected serum lipid levels [27,28]. Future research on the relationship between ACAT1 gene polymorphisms and stage of liver fibrosis in human subjects may be needed to diagnose susceptibility to liver fibrosis.

In summary, we propose a new mechanistic model linking ACAT1 and liver fibrosis. Our results suggest new therapeutic interventions directed at ACAT1 activities in HSCs could improve treatment of liver fibrosis.

Financial support

This study was supported by a Grant-in-Aid for Japan Research Foundation for Clinical Pharmacology, Takeda Science Foundation, Suzuken Memorial Foundation, and Scientific Research from the Ministry of Education, Culture, Sports, Science, and Technology of Japan.

Conflict of interest

The authors who have taken part in this study declared that they do not have anything to disclose regarding funding or conflict of interest with respect to this manuscript.

Acknowledgments

The authors thank Mina Kitazume and Miho Takabe (Keio University) for helpful advice and technical assistance.

Supplementary data

Supplementary data associated with this article can be found, in the online version, at http://dx.doi.org/10.1016/j.jhep.2014.03.018.

References

[1] Bataller R, Brenner DA. Liver fibrosis. J Clin Invest 2005;115:209–218.
[2] Lee UE, Friedman SL. Mechanisms of hepatic fibrogenesis. Best Pract Res Clin Gastroenterol 2011;25:195–206.
[3] Teratani T, Tomita K, Suzuki T, Oshikawa T, Yokoyama H, Shimamura K, et al. A high-cholesterol diet exacerbates liver fibrosis in mice via accumulation of free cholesterol in hepatic stellate cells. Gastroenterology 2012;142:e110.
[4] Chang TY, Li BL, Chang CC, Urano Y. Acyl-coenzyme A:cholesterol acyltransferases. Am J Physiol Endocrinol Metab 2009;297:E1–E9.
[5] Bataller R, Sancho-Bru P, Gines P, Lora JM, Al-Garawi A, Sole M, et al. Activated human hepatic stellate cells express the renin-angiotensin system and synthesize angiotensin II. Gastroenterology 2003;125:117–125.
[6] Tomita K, Tamiya G, Ando S, Ohsumi K, Chiyo T, Mizutani A, et al. Tumour necrosis factor alpha signalling through activation of Kupffer cells plays an essential role in liver fibrosis of non-alcoholic steatohepatitis in mice. Gut 2006;55:415–424.
[7] Tomita K, Azuma T, Kitamura N, Nishida J, Tamiya G, Oka A, et al. Pioglitazone prevents alcohol-induced fatty liver in rats through up-regulation of c-Met. Gastroenterology 2004;126:873–885.
[8] Chang CC, Sakashita N, Ornvold K, Lee O, Chang ET, Dong R, et al. Immunological quantitation and localization of ACAT-1 and ACAT-2 in human liver and small intestine. J Biol Chem 2000;275:28083–28092.
[9] Xu L, Hui AY, Albanis E, Arthur MJ, O'Byrne SM, Blaner WS, et al. Human hepatic stellate cell lines, LX-1 and LX-2: new tools for analysis of hepatic fibrosis. Gut 2005;54:142–151.
[10] Schnabl B, Choi YH, Olsen JC, Hagedorn CH, Brenner DA. Immortal activated human hepatic stellate cells generated by ectopic telomerase expression. Lab Invest 2002;82:323–333.
[11] Su GL. Lipopolysaccharides in liver injury: molecular mechanisms of Kupffer cell activation. Am J Physiol Gastrointest Liver Physiol 2002;283:G256–G265.
[12] Husebye H, Halaas O, Stenmark H, Tunheim G, Sandanger O, Bogen B, et al. Endocytic pathways regulate Toll-like receptor 4 signaling and link innate and adaptive immunity. EMBO J 2006;25:683–692.
[13] Wang Y, Chen T, Han C, He D, Liu H, An H, et al. Lysosome-associated small Rab GTPase Rab7b negatively regulates TLR4 signaling in macrophages by promoting lysosomal degradation of TLR4. Blood 2007;110:962–971.
[14] Mandal SK, Iakhiaev A, Pendurthi UR, Rao LV. Acute cholesterol depletion impairs functional expression of tissue factor in fibroblasts: modulation of tissue factor activity by membrane cholesterol. Blood 2005;105:153–160.
[15] Seki E, De Minicis S, Osterreicher CH, Kluwe J, Osawa Y, Brenner DA, et al. TLR4 enhances TGF-beta signaling and hepatic fibrosis. Nat Med 2007;13:1324–1332.
[16] Chang TY, Chang CC, Ohgami N, Yamauchi Y. Cholesterol sensing, trafficking, and esterification. Annu Rev Cell Dev Biol 2006;22:129–157.
[17] Meuwese MC, de Groot E, Duivenvoorden R, Trip MD, Ose L, Maritz FJ, et al. ACAT inhibition and progression of carotid atherosclerosis in patients with familial hypercholesterolemia: the CAPTIVATE randomized trial. JAMA 2009;301:1131–1139.
[18] Nissen SE, Tuzcu EM, Brewer HB, Sipahi I, Nicholls SJ, Ganz P, et al. Effect of ACAT inhibition on the progression of coronary atherosclerosis. N Engl J Med 2006;354:1253–1263.
[19] Accad M, Smith SJ, Newland DL, Sanan DA, King Jr LE, Linton MF, et al. Massive xanthomatosis and altered composition of atherosclerotic lesions in hyperlipidemic mice lacking acyl CoA:cholesterol acyltransferase 1. J Clin Invest 2000;105:711–719.
[20] Fazio S, Major AS, Swift LL, Gleaves LA, Accad M, Linton MF, et al. Increased atherosclerosis in LDL receptor-null mice lacking ACAT1 in macrophages. J Clin Invest 2001;107:163–171.
[21] Su YR, Dove DE, Major AS, Hasty AH, Boone B, Linton MF, et al. Reduced ABCA1-mediated cholesterol efflux and accelerated atherosclerosis in apolipoprotein E-deficient mice lacking macrophage-derived ACAT1. Circulation 2005;111:2373–2381.
[22] Dove DE, Su YR, Zhang W, Jerome WG, Swift LL, Linton MF, et al. ACAT1 deficiency disrupts cholesterol efflux and alters cellular morphology in macrophages. Arterioscler Thromb Vasc Biol 2005;25:128–134.
[23] Maxfield FR, Tabas I. Role of cholesterol and lipid organization in disease. Nature 2005;438:612–621.
[24] Feng B, Yao PM, Li Y, Devlin CM, Zhang D, Harding HP, et al. The endoplasmic reticulum is the site of cholesterol-induced cytotoxicity in macrophages. Nat Cell Biol 2003;5:781–792.
[25] Dickhout JG, Colgan SM, Lhotak S, Austin RC. Increased endoplasmic reticulum stress in atherosclerotic plaques associated with acute coronary syndrome: a balancing act between plaque stability and rupture. Circulation 2007;116:1214–1216.

[26] Youm YH, Kanneganti TD, Vandanmagsar B, Zhu X, Ravussin A, Adijiang A, et al. The Nlrp3 inflammasome promotes age-related thymic demise and immunosenescence. Cell Rep 2012;1:56–68.
[27] Wu DF, Yin RX, Aung LH, Li Q, Yan TT, Zeng XN, et al. Sex-specific association of ACAT-1 rs1044925 SNP and serum lipid levels in the hypercholesterolemic subjects. Lipids Health Dis 2012;11:9.
[28] Ohta T, Takata K, Katsuren K, Fukuyama S. The influence of the acyl-CoA:cholesterol acyltransferase-1 gene (−77G −>A) polymorphisms on plasma lipid and apolipoprotein levels in normolipidemic and hyperlipidemic subjects. Biochim Biophys Acta 2004;1682:56–62.

OPEN

Citation: Oncogenesis (2014) 3, e104; doi:10.1038/oncsis.2014.17

www.nature.com/oncsis

ORIGINAL ARTICLE

Inhibitors of enhancer of zeste homolog 2 (EZH2) activate tumor-suppressor microRNAs in human cancer cells

S Hibino, Y Saito, T Muramatsu, A Otani, Y Kasai, M Kimura and H Saito

Enhancer of zeste homolog 2 (EZH2) enhances tumorigenesis and is commonly overexpressed in several types of cancer. To investigate the anticancer effects of EZH2 inhibitors, microRNA (miRNA) expression profiles were examined in gastric and liver cancer cells treated with suberoylanilide hydroxamic acid (SAHA) and 3-deazaneplanocin A (DZNep). We confirmed that SAHA and DZNep suppressed EZH2 expression in AGS and HepG2 cells and inhibited their proliferation. The results of microarray analyses demonstrated that *miR-1246* was commonly upregulated in cancer cells by treatment with SAHA and DZNep. *MiR-302a* and *miR-4448* were markedly upregulated by treatment with SAHA and DZNep, respectively. DYRK1A, CDK2, BMI-1 and Girdin, which are targets of *miR-1246*, *miR-302a* and *miR-4448*, were suppressed by treatment with SAHA and DZNep, leading to apoptosis, cell cycle arrest and reduced migration of AGS and HepG2 cells. ChIP assay revealed that SAHA and DZNep inhibited the binding of EZH2 to the promoter regions of *miR-1246*, *miR-302a* and *miR-4448*. These findings suggest that EZH2 inhibitors such as SAHA and DZNep exert multiple anticancer effects through activation of tumor-suppressor miRNAs.

Oncogenesis (2014) **3,** e104; doi:10.1038/oncsis.2014.17; published online 26 May 2014

Subject Categories: Tumour suppression

Keywords: EZH2; microRNA; SAHA; DZNep; cancer

INTRODUCTION

Epigenetic silencing of tumor-suppressor genes in human cancer is mediated by aberrant DNA methylation and histone modification. The polycomb repressive complex 2 mediates epigenetic gene silencing by trimethylating histone H3 lysine 27 and is known to aberrantly silence tumor-suppressor genes in cancer. Enhancer of zeste homolog 2 (EZH2), which is the catalytic subunit of polycomb repressive complex 2, enhances tumorigenesis and is commonly overexpressed in several types of cancer.[1] Moreover, EZH2 has been reported to have an essential role in self-renewal of cancer stem cells,[2] indicating that EZH2-targeting drugs can act as potent anticancer agents.

Epigenetic therapy with DNA methylation inhibitors and histone-modifying drugs has emerged as an effective approach for chemotherapy as well as chemoprevention of cancer. The histone deacetylase (HDAC) inhibitor suberoylanilide hydroxamic acid (SAHA) has been approved for patients with cutaneous T-cell lymphoma.[3] Recently, it was discovered that 3-deazaneplanocin A (DZNep) inhibits EZH2, which has H3K27 trimethylation activity.[4] Although SAHA is widely accepted as an HDAC inhibitor, it has been reported to suppress EZH2 expression in cancer cells and to exert an anticancer effect, indicating that SAHA also functions as an EZH2 inhibitor.[5,6]

MicroRNAs (miRNAs) are small noncoding RNAs that function as endogenous silencers of various target genes. Specific miRNAs such as *miR-34a* are downregulated in various cancers and act as tumor suppressors. On the other hand, miRNAs such as *miR-155* and the *miR-17-92* cluster are reportedly overexpressed in various cancers, and act as oncogenes.[7–11] Aberrant expression of miRNAs has a critical role in human carcinogenesis. We have discovered that some miRNAs including *miR-127* are regulated by epigenetic alterations such as DNA methylation and histone modification.[12] DNA methylation inhibitors and HDAC inhibitors can activate epigenetically silenced tumor-suppressor miRNAs accompanied by downregulation of target oncogenes in human cancer cells.[12,13] However, the miRNA expression profiles altered by EZH2 inhibitors are still unknown. In the present study, to investigate the molecular mechanisms underlying the anticancer effects of EZH2 inhibitors, miRNA expression profiles in gastric and liver cancer cells were analyzed after treatment with SAHA and DZNep.

RESULTS

SAHA and DZNep inhibit EZH2 expression in, and proliferation of, AGS and HepG2 cells

We first investigated the levels of EZH2 expression and the antiproliferative activity of SAHA and DZNep in AGS and HepG2 cells. As shown in Figure 1, EZH2 expression in both AGS and HepG2 cells was suppressed by treatment with 1 μM SAHA and 5 μM DZNep for 72 h. The numbers of AGS and HepG2 cells were significantly reduced 72 h after treatment with SAHA and DZNep. These findings suggest that both AGS and HepG2 cells are sensitive to SAHA and DZNep, and that these histone-modifying drugs inhibit EZN2 expression and the proliferative activity of cancer cells derived from the stomach and the liver.

We also examined the alteration of stemness in AGS and HepG2 cells using a sphere-forming assay. Under anchorage-independent stem cell-specific culture conditions, AGS and HepG2 cells formed spheroids, as shown in Figure 2a. Treatment with SAHA and DZNep significantly reduced the number of these spheroids. The

Division of Pharmacotherapeutics, Keio University Faculty of Pharmacy, Minato-ku, Tokyo, Japan. Correspondence: Dr Y Saito, Division of Pharmacotherapeutics, Keio University Faculty of Pharmacy, 1-5-30 Shibakoen, Minato-ku, Tokyo 105-8512, Japan.
E-mail: saito-ys@pha.keio.ac.jp
Received 12 February 2014; revised 28 March 2014; accepted 10 April 2014

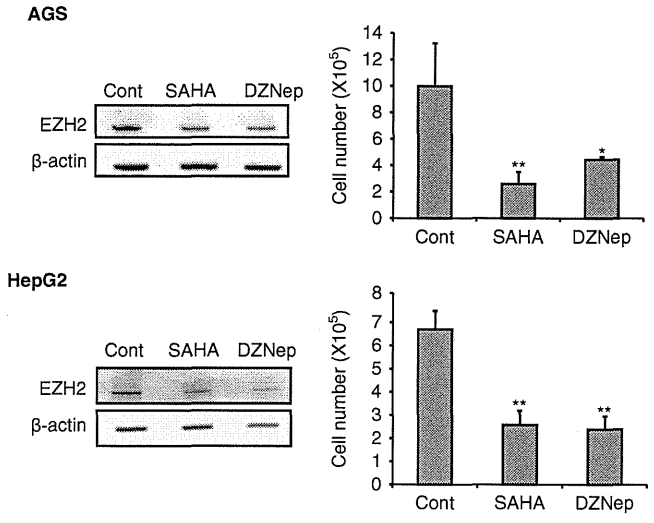

Figure 1. EZH2 expression and proliferation of cancer cells treated with SAHA and DZNep. Western blotting of EZH2 and cell counting assay were performed in AGS and HepG2 cells treated with SAHA and DZNep. *$P<0.01$, **$P<0.001$.

levels of expression of *Oct3/4* and *Sox2*, which are essential for induction of pluripotent stem (iPS) cells, were significantly increased in AGS and HepG2 cells after spheroid formation. These results suggest that SAHA and DZNep suppress the stemness of AGS and HepG2 cells (Figure 2b).

miR-1246 is a common target of EZH2 inhibitors in cancer cells

To investigate the miRNA expression profiles altered by the treatment of AGS and HepG2 cells with SAHA and DZNep, we conducted microarray analyses. miRNAs that were significantly upregulated after treatment of AGS and HepG2 cells with SAHA and DZNep are summarized in Table 1. Interestingly, *miR-1246* was upregulated in both cell lines after SAHA and DZNep treatment (Table 1). Increased expression of *miR-1246* by treatment with SAHA and DZNep was confirmed by quantitative RT–PCR (Figure 3a). This suggests that *miR-1246* is a common target of SAHA and DZNep in cancer cells and can be activated by these histone-modifying drugs.

miR-302a and *miR-4448* are upregulated by SAHA and DZNep

We also found that *miR-302a* and *miR-4448* were most upregulated by treatment of AGS cells with SAHA, and by treatment of both AGS and HepG2 cells with DZNep, respectively (Table 1). Upregulation of *miR-302a* and *miR-4448* by treatment with SAHA and DZNep was confirmed by quantitative RT–PCR (Figures 2b and c). Recent studies have shown that *miR-302* is the major miRNA found in human embryonic stem cells and iPS cells, and that induction of *miR-302* expression reprograms somatic cells into a pluripotent stem cell-like state.[14,15] *MiR-302* has been reported to inhibit the tumorigenicity of human pluripotent stem cells and the proliferation of cervical carcinoma cells.[16,17] Although *miR-4448* was identified only recently and its function is still unclear, we focused our study on *miR-4448*, as it was robustly induced by DZNep treatment.

miR-1246, *miR-302a* and *miR-4448* suppress their target genes upon treatment with SAHA and DZNep in cancer cells

A recent study has shown that dual-specificity tyrosine phosphorylation-regulated kinase 1A (DYRK1A), a Down syndrome-associated protein kinase, is a target of *miR-1246*.[18] We examined the levels of expression of *miR-1246* and its target DYRK1A by quantitative RT–PCR and western blotting, respectively. As shown in Figure 3a, the expression level of *miR-1246* was increased, and accompanied by downregulation of DYRK1A, after treatment of AGS and HepG2 cells with SAHA and DZNep. Cyclin-dependent kinase 2 (CDK2) and BMI-1 polycomb ring finger oncogene (BMI-1), both of which are known to be cell cycle regulators, have been identified as targets of *miR-302*.[16] Figure 3b shows the expression levels of *miR-302a* and its targets CDK2 and BMI-1. *MiR-302a* was significantly upregulated in comparison with control cells, and CDK2 and BMI-1 were downregulated, after treatment of AGS cells with SAHA and DZNep.

To investigate whether *miR-4448* targets any cancer-related genes, we searched the miRNA-target databases Targetscan (http://www.targetscan.org/vert_61/) and miRDB (http://mirdb.org/miRDB/). These databases strongly implicate CCDC88A (coiled-coil domain containing 88A, also known as Girdin) as a candidate target gene of *miR-4448* with high scores. Girdin is a component of the phosphatidylinositol 3-kinase (PI3-K)/Akt pathway, which is a pivotal signaling pathway for cancer progression and has an important role in cancer cell migration by controlling actin organization.[19] As shown in Figure 3c, expression of Girdin protein was reduced after DZNep treatment in both AGS and HepG2 cells, and this was accompanied by upregulation of *miR-4448* expression.

SAHA and DZNep induce apoptosis and cell cycle (G1/S) arrest in AGS and HepG2 cells and inhibit their migration

To elucidate the molecular mechanism underlying the suppression of cancer cells by histone-modifying drugs, we conducted Annexin V-FITC apoptosis assay and cell cycle assay. As shown in Figure 4a, flow cytometry analyses revealed that Annexin V-positive cells were increased among both AGS and HepG2 cells after treatment with SAHA and DZNep, indicating that these histone-modifying drugs induce apoptosis of cancer cells. Figure 4b shows the results of the cell cycle assay in which AGS and HepG2 cells were treated with histone-modifying drugs. The proportion of AGS cells in G1-phase was increased after treatment with SAHA and DZNep, suggesting induction of G1/S arrest. On the other hand, the proportion of HepG2 cells in sub-G1-phase was increased after treatment with SAHA and DZNep, suggesting induction of apoptosis by these drugs.

As Girdin, which is associated with cancer cell migration, was downregulated by DZNep treatment, we conducted the wound-healing assay, which is a standard assay for measuring cell migration. As shown in Figure 5, after DZNep treatment, the wound width of plated AGS and HepG2 cells was significantly increased, and the number of migrated AGS cells was significantly suppressed. These results suggest that DZNep suppresses the migration of AGS and HepG2 cells.

Binding of EZH2 to the promoter regions of *miR-1246*, *miR-302a* and *miR-4448* is inhibited by SAHA and DZNep

Finally, we performed the ChIP assay with antibodies against EZH2 and p53 to clarify the mechanism responsible for regulation of these miRNAs by histone-modifying drugs. Chromatin around the *miR-1246* promoter region that was immunoprecipitated with EZH2 antibody was significantly reduced by treatment with SAHA and DZNep in both AGS and HepG2 cells (Figure 6a). A recent study has shown that *miR-1246* has a p53-responsive element in its promoter region, and that p53 induces *miR-1246* expression in response to DNA damage.[18] The results of the ChIP assay demonstrate that binding of p53 to the *miR-1246* promoter region was significantly increased by treatment of cancer cells with SAHA and DZNep (Figure 6a).

Chromatin around the *miR-302a* promoter region that was immunoprecipitated with EZH2 antibody was significantly

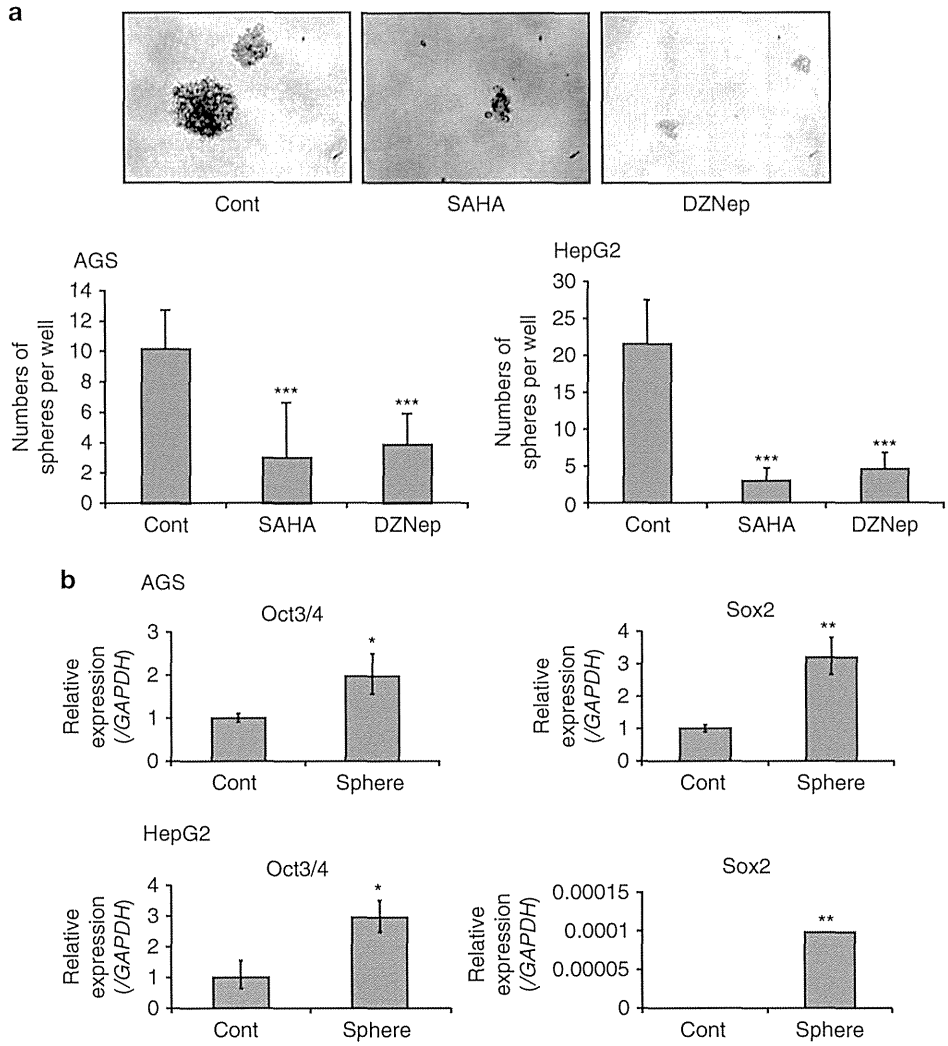

Figure 2. Alteration of stemness in cancer cells after treatment with EZH2 inhibitors. (**a**) Sphere-forming assay of AGS and HepG2 cells treated with SAHA and DZNep. Under anchorage-independent stem cell-specific culture conditions, AGS and HepG2 cells form spheroids. Spheroids derived from AGS cells are shown. The number of spheres derived from AGS and HepG2 cells treated with SAHA and DZNep was compared with control cells. ***$P<0.001$. (**b**) Quantitative RT-PCR of *Oct3/4* and *Sox2* in spheroids of AGS and HepG2 cells. Relative expression of *Oct3/4* and *Sox2* in spheres derived from AGS and HepG2 cells was compared with that of control cells. For control of *Oct3/4* and *Sox2* expression after spheroid formation, we used AGS or HepG2 cells cultured in regular media supplemented with 10% FBS. *$P<0.05$, **$P<0.01$.

reduced by treatment with SAHA and DZNep in AGS cells (Figure 6b). As for *miR-4448*, we examined the potential promoter region located on chromosome 3: 183602504-183602724. Binding of EZH2 to the potential *miR-4448* promoter was significantly decreased after DZNep treatment in AGS cells. Unexpectedly, in HepG2 cells, binding of EZH2 was increased after DZNep treatment (Figure 6c). These findings indicate that binding of EZH2 to the promoter regions of *miR-1246*, *miR-302a* and *miR-4448* was inhibited in cancer cells by treatment with SAHA and DZNep.

DISCUSSION

Drugs that target chromatin-modifying enzymes such as DNA methylation inhibitors and HDAC inhibitors hold clinical promise for treatment of cancer. However, the molecular mechanisms underlying the anticancer effects of EZH2 inhibitors are not fully understood. DZNep inhibits EZH2, which exerts trimethylation activity on H3K27. SAHA is widely accepted as an HDAC inhibitor, but its function as an EZH2 inhibitor has also been reported.[5,6] Recent studies have shown that EZH2 interacts with HDACs via EED (embryonic ectoderm development: as one of the polycomb repressive complex 2 component proteins) and that EZH2-mediated gene silencing is dependent on HDAC activity.[20] In addition, another HDAC inhibitor, trichostatin A, completely abrogates the effects of EZH2 overexpression in cancer cells, thus supporting the function of SAHA as an EZH2 inhibitor.[21]

Here we have shown for the first time that, in cancer cells, *miR-1246* is a common target of EZH2 inhibitors and that *miR-302a* and *miR-4448* are activated by SAHA and DZNep. Our results demonstrate that SAHA and DZNep suppress EZH2 expression and activate tumor-suppressor miRNAs in cancer cells. ChIP assay revealed that binding of EZH2 to the promoter regions of *miR-1246*, *miR-302a* and *miR-4448* was inhibited by SAHA and DZNep. As EZH2 is the catalytic subunit of polycomb repressive complex 2, which mediates epigenetic gene silencing by trimethylating histone H3 lysine 27, suppression of EZH2 by SAHA and DZNep may induce transcriptional activation of *miR-1246*, *miR-302a* and *miR-4448* in cancer cells. In HepG2 cells, binding of EZH2 to the putative *miR-4448* promoter region was not suppressed by DZNep, suggesting that *miR-4448* expression is not under the direct

Table 1. MiRNA expression profiles in AGS and HepG2 cells treated with SAHA and DZNep

	AGS-SAHA				*HepG2-SAHA*		
	Cont	*SAHA*	*Ratio*		*Cont*	*SAHA*	*Ratio*
**miR-302a*	28.4	410.6	14.4	*miR-301a*	32.3	258.7	8.0
miR-205	19.7	210.0	10.7	*miR-16*	177.5	1187.2	6.7
miR-1915	34.3	300.2	8.8	*miR-4286*	3189.0	20115.4	6.3
miR-146b-5p	38.1	265.3	7.0	*miR-378c*	28.5	158.0	5.5
miR-188-5p	21.5	143.8	6.7	*miR-107*	649.3	3513.9	5.4
miR-221	139.6	896.9	6.4	*miR-103*	895.0	4614.8	5.2
miR-663	84.5	532.5	6.3	*miR-18a*	91.7	470.1	5.1
miR-2861	325.6	1860.0	5.7	*miR-125a-3p*	107.7	540.7	5.0
miR-181a	57.0	320.7	5.6	*miR-15a*	31.5	155.0	4.9
miR-3196	437.5	2322.5	5.3	*miR-378*	61.1	281.4	4.6
miR-1469	73.2	383.6	5.2	*miR-422a*	52.7	187.4	3.6
miR-3621	210.6	1079.1	5.1	*miR-21**	39.2	135.9	3.5
miR-3180	45.3	229.9	5.1	*miR-19b*	349.3	1126.3	3.2
miR-3656	295.0	1469.4	5.0	*miR-22*	501.9	1609.3	3.2
miR-1908	221.2	1083.9	4.9	*miR-532-5p*	34.9	107.4	3.1
miR-4294	63.6	310.7	4.9	*miR-660*	53.3	159.7	3.0
miR-1268	124.4	590.8	4.7	**miR-1246*	2438.0	7229.7	3.0
miR-3195	34.9	164.1	4.7	*miR-185*	95.6	268.3	2.8
miR-193b	37.0	173.2	4.7	*miR-425*	216.4	591.1	2.7
miR-3665	575.6	2686.4	4.7	*miR-1260b*	17758.0	46685.1	2.6
miR-23a	801.3	3358.3	4.2	*miR-4284*	8795.4	22991.7	2.6
**miR-1246*	820.5	3435.9	4.2	*miR-128*	74.2	193.0	2.6
miR-373	5716.4	23818.2	4.2	*miR-194*	1072.3	2787.3	2.6
miR-4327	36.3	149.3	4.1				
miR-638	242.2	989.9	4.1				
miR-762	547.8	2226.8	4.1				
	AGS-DZNep				*HepG2-DZNep*		
	Cont	*DZNep*	*Ratio*		*Cont*	*DZNep*	*Ratio*
**miR-4448*	64.2	2725.7	42.4	**miR-4448*	72.5	592.9	8.2
miR-3676	41.1	160.7	3.9	*miR-4485*	226.5	956.1	4.2
miR-221	141.9	393.5	2.8	*miR-4294*	95.0	339.2	3.6
**miR-1246*	834.2	2299.4	2.8	*miR-3676*	120.4	416.2	3.5
miR-3131	35.4	93.4	2.6	*miR-4419b*	13.8	46.8	3.4
miR-3194-5p	14.4	34.9	2.4	*miR-4725-3p*	103.0	339.7	3.3
miR-940	20.4	47.8	2.3	**miR-1246*	5544.7	17245.6	3.1
miR-4730	45.7	99.6	2.2	*miR-1290*	144.0	443.1	3.1
miR-4745-5p	71.9	148.2	2.1	*miR-4675*	20.0	58.3	2.9
				miR-146b-5p	61.6	179.1	2.9

Signal intensities and their ratios in microarray analyses are shown. MiR-1246, miR-302a and miR-4448 are indicated by asterisks.

control of EZH2. Transcription factors regulated by EZH2 may control *miR-4448* expression in liver cancer cells. In addition, *miR-1246* has a p53-responsive element in its promoter region, and p53 induces *miR-1246* expression.[18] Treatment with SAHA and DZNep increased p53 binding to the *miR-1246* promoter region, thus further increasing *miR-1246* expression.

DYRK1A, which was recently identified as one of the targets of *miR-1246*, was significantly suppressed by treatment with EZH2 inhibitors, resulting in apoptosis of AGS and HepG2 cells. DYRK1A has been shown to suppress caspase-9-mediated apoptosis in mammalian cells through phosphorylation of caspase-9 on threonine residue 125.[22,23] These findings suggest that SAHA and DZNep induce DYRK1A-mediated apoptosis in cancer cells through activation of *miR-1246*. Treatment of AGS cells with DZNep and SAHA suppressed CDK2 and BMI-1, which were recently identified as the targets of *miR-302*, and induced cell cycle (G1/S) arrest. CDK2 is a G1-phase checkpoint regulator, and its suppression may result in inhibition of G1–S cell cycle transition pathways. Deficiency of BMI-1, an oncogenic cancer stem cell marker, has been shown to inhibit G1–S cell cycle transition through enhancement of p16Ink4a and p14Arf tumor-suppressor activities.[24] Thus, concurrent silencing of CDK2 and BMI-1 by *miR-302a* may synergistically bring about G1/S cell cycle arrest of AGS cells. We also found that treatment with DZNep suppressed the expression of Girdin and inhibited the migration of AGS and HepG2 cells, probably because of the activation of *miR-4448*. It has been reported previously that Girdin is highly expressed in a variety of human cancers and that shRNA knockdown of Girdin markedly inhibits the metastasis of breast cancer cells.[25] These findings suggest that DZNep may impair progression of cancer and migration of cancer cells by suppression of Girdin through activation of *miR-4448*.

In the present study, we focused on three miRNAs—*miR-1246*, *miR-302a* and *miR-4448*—which were robustly upregulated by SAHA and DZNep treatment in AGS and HepG2 cells. However, other miRNAs listed in Table 1 are also associated with apoptosis and migration of cancer cells. For example, it has been reported that *miR-15*, *miR-16* and *miR-181a* induce apoptosis of cancer cells by targeting *BCL2*[26–28] and that *miR-205* inhibits the migration of cancer cells.[29,30] In addition, recent studies have shown that *miR-1915* also targets *BCL2* and has an important role in the development of multidrug resistance in colorectal carcinoma cells[31] and that *miR-146b-5p* reduces migration and invasion of glioma by targeting epidermal growth factor receptor and matrix metalloproteinase 16.[32,33] On the other hand, several potential oncogenic miRNAs such as *miR-21*, *miR-103* and *miR-221* are also

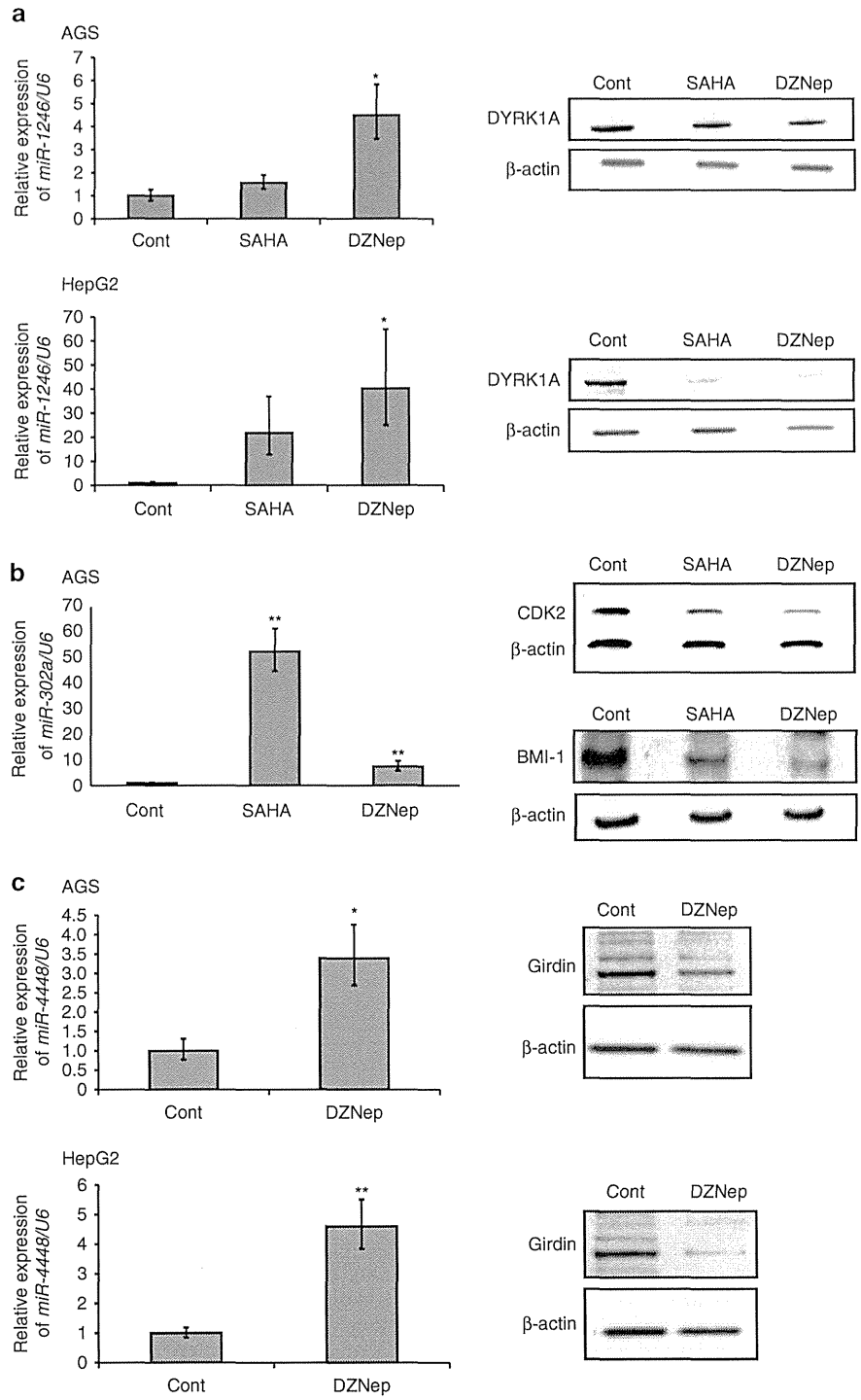

Figure 3. Expression levels of *miR-1246*, *miR-302a* and *miR-4448* and their target genes in AGS and HepG2 cells treated with EZH2 inhibitors. (**a**) Quantitative RT-PCR of *miR-1246* and western blotting of DYRK1A in AGS and HepG2 cells treated with SAHA and DZNep. $^{*}P<0.05$. (**b**) Quantitative RT-PCR of *miR-302a* and western blotting of CDK2 and BMI-1 in AGS cells treated with SAHA and DZNep. $^{**}P<0.01$. (**c**) Quantitative RT-PCR of *miR-4448* and western blotting of Girdin in AGS and HepG2 cells treated with DZNep. $^{*}P<0.05$, $^{**}P<0.01$.

upregulated after treatment with SAHA and DZNep.[34–37] In particular, *miR-221* promotes tumorigenesis of gastric and liver cancer cells by targeting tumor-suppressor genes such as *PTEN*.[35,36] Gebeshuber *et al.*[38] have proposed that whether one miRNA acts as a tumor suppressor or oncogene is largely dependent on cell condition. Further studies are needed to examine how these potential oncogenic miRNAs are implicated in the anticancer effect of EZH2 inhibitors.

As EZH2 has been reported to be essential for self-renewal of cancer stem cells,[2] SAHA and DZNep, which inhibit EZH2, could be promising therapeutic agents for suppression of cancer stem cells.[39,40] After culture of AGS and HepG2 cells under anchorage-independent stem cell-specific conditions, spheroids were formed, as shown in Figure 2a. The stem cell properties of the spheroid-forming cells were confirmed by upregulation of *Oct3/4* and *Sox2*, which are essential for iPS cells. SAHA and DZNep significantly

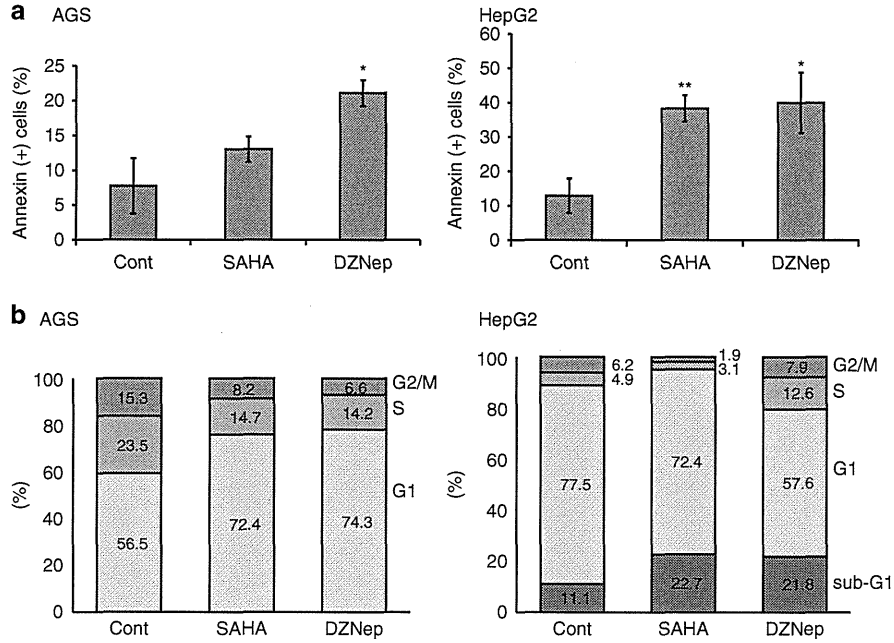

Figure 4. Apoptosis and cell cycle assays of AGS and HepG2 cells treated with EZH2 inhibitors. (**a**) Annexin V apoptosis assay of AGS and HepG2 cells treated with SAHA and DZNep. $*P<0.01$, $**P<0.001$. (**b**) Cell cycle assay of AGS and HepG2 cells treated with SAHA and DZNep.

inhibited spheroid formation, suggesting that EZH2 inhibitors suppress the stemness of AGS and HepG2 cells. Other studies have also shown that EZH2 inhibitors act against the cancer stem cell population in pancreatic cancer and glioblastoma.[39–41] These findings indicate that EZH2 inhibitors may be promising agents for cancer stem cell-targeting therapy.

Accumulating evidence has revealed that the *miR-302-367* cluster is deeply associated with stemness in pluripotent cells, but we and other groups have shown that the *miR-302-367* cluster also acts as a potent tumor suppressor in cancer stem cells. Fareh *et al.*[42] have reported that the *miR-302-367* cluster has an ability to suppress the cancer-stemness signature of glioma-initiating cells. In addition, recent studies have reported that the *miR-520* cluster, which is overexpressed in human ES cells, also acts as a tumor suppressor, and that introduction of *miR-520h* mimics into pancreatic cancer cells results in reduction of side population cells.[43,44] In general, miRNAs have multiple functions in response to different cell conditions through suppression of various target genes. Our results suggest that *miR-302a* acts as a tumor suppressor and suppresses the cancer-stemness signature in cancer cells by suppressing target genes such as *CDK2* and *BMI-1*, although it has an important role in maintaining stemness in pluripotent cells such as ES cells and iPS cells.

Figure 7 summarizes our present findings. In cancer cells, tumor-suppressor miRNAs are silenced by a repressive chromatin structure involving trimethylating histone H3 lysine 27 mediated by chromatin-modifying factors including EZH2. Treatment with SAHA and/or DZNep suppresses EZH2 expression and reduces the level of H3K27 methylation, creating a more active chromatin structure, and thus allowing p53 to bind to the promoter region of *miR-1246*. Tumor-suppressor miRNAs such as *miR-1246*, *miR-302a* and *miR-4448* are activated and suppress their cancer-related target genes, thus inducing apoptosis and G1/S arrest of cancer cells and inhibiting their migration. In conclusion, EZH2 inhibitors such as SAHA and DZNep exert multiple anticancer effects through activation of tumor-suppressor miRNAs in human cancer cells. Epigenetic therapy with EZH2 inhibitors holds clinical promise for the management of human malignancies.

MATERIALS AND METHODS

Cell culture and drug treatment

AGS, a human gastric cancer cell line, was obtained from the American Type Culture Collection (Rockville, MD, USA) and cultured in RPMI1640 medium supplemented with 10% fetal bovine serum (FBS). HepG2, a human liver cancer cell line, was obtained from RIKEN Cell Bank (Tsukuba, Japan) and cultured in Dulbecco's Minimal Essential Medium supplemented with 10% FBS. For drug treatment, cells were seeded the day before drug administration, and then treated with 5 μM DZNep (Cayman Chemical, Ann Arbor, MI, USA) or 1 μM SAHA (Sigma-Aldrich, St Louis, MO, USA) for 72 h.[45,46]

Cell counting

AGS and HepG2 cells were seeded at 1.0×10^5 cells per well in a 6-well plate. AGS and HepG2 cells were cultured in media supplemented with 10% FBS and treated with 1 μM SAHA and 5 μM DZNep for 72 h. After treatment with DZNep and SAHA, the cells were counted using a Cellometer (Tomy Digital Biology, Tokyo, Japan). The data are indicated as mean ± s.d. from three independent experiments.

RNA extraction and microarray analysis

Total RNAs were extracted from cancer cell lines using the mirVana miRNA isolation kit (Applied Biosystems, Foster City, CA, USA). MiRNA microarray analyses were conducted by Toray Industries (www.toray.com: Tokyo, Japan). This microarray chip contains probe regions that detect 1719 miRNA transcripts listed in Sanger miRBase Release 17.0 (http://www.sanger.ac.uk). The average values of the various miRNA signal intensities detected by the chip were then compared.

Quantitative RT–PCR

Expression levels of genes were analyzed by TaqMan quantitative RT–PCR assay for *miR-1246*, *miR-302a*, *Oct3/4* and *Sox2* (Applied Biosystems) in accordance with the manufacturer's instructions. Quantitative analysis was performed using the CFX96 Real-Time System (BioRad, Hercules, CA, USA). *U6* was used as an internal control for *miR-1246* and *miR-302a*. *GAPDH* was used as an internal control for *Oct3/4* and *Sox2*. For control of *Oct3/4* and *Sox2* expression after spheroid formation, we used AGS or HepG2 cells cultured in regular media supplemented with 10% FBS. Experiments were carried out in triplicate.

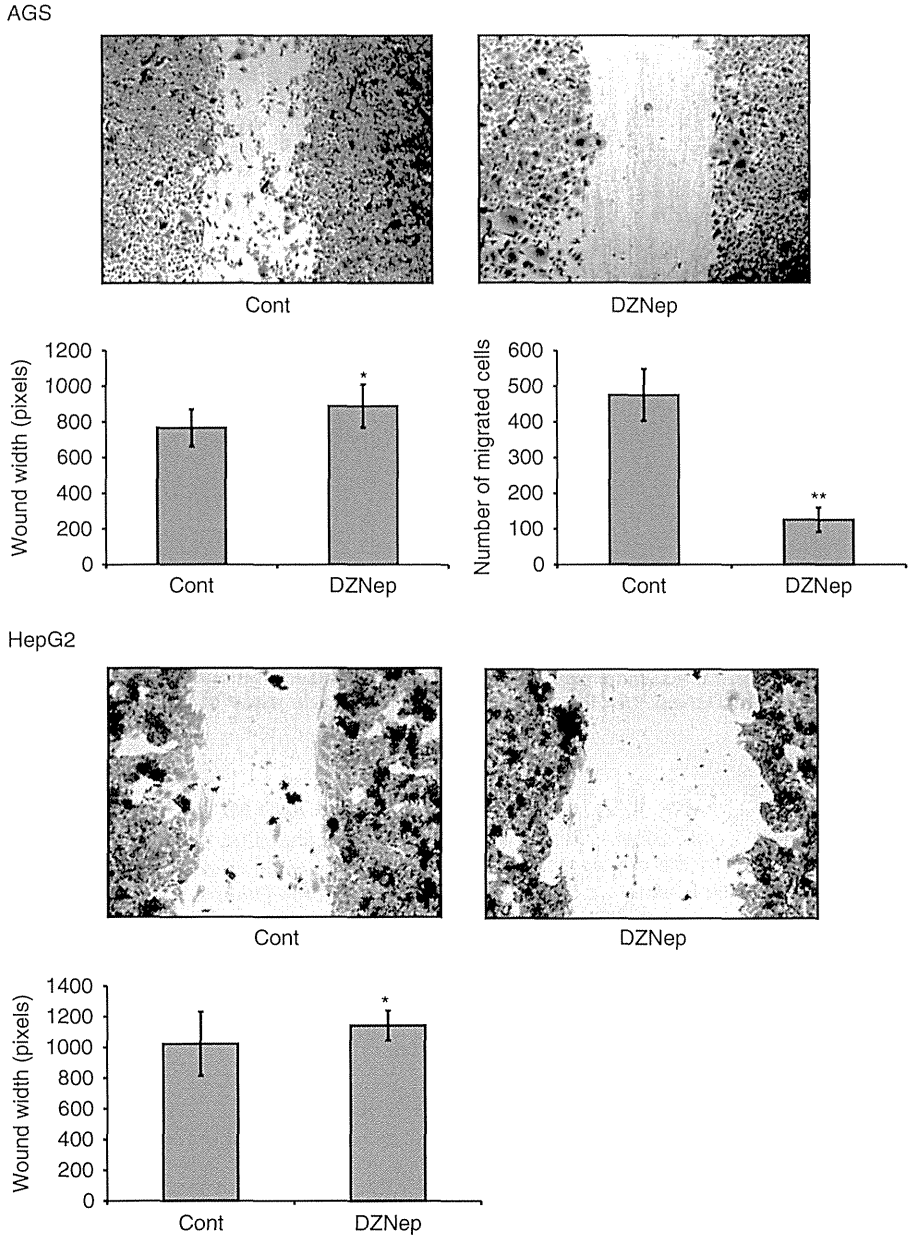

Figure 5. Wound-healing assay of AGS and HepG2 cell migration after treatment with DZNep. Wound healing of AGS and HepG2 cells is shown. Wound width of plated AGS and HepG2 cells after DZNep treatment was compared with that of control cells. The number of migrated AGS cells after treatment with DZNep was compared with that of control cells. $^{*}P<0.05$, $^{**}P<0.01$.

Antibodies

Antibodies against Girdin (T-13) and CDK2 (SC-163) were purchased from Santa Cruz Biotechnology (Dallas, TX, USA). Antibodies against DYRK1A (Cell Signaling, Danvers, MA, USA), EZH2 (BD Biosciences, San Jose, CA, USA) and BMI-1 (Abcam, Cambridge, UK) were used. HRP-conjugated β-actin (Santa Cruz Biotechnology) was used as an internal control for western blotting. ChIP Ab+ EZH2 (Millipore, Billerica, MA, USA) and p53 antibody (Cell Signaling) were used for the ChIP assay.

Chromatin immunoprecipitation (ChIP) assay

The ChIP assay was performed as described previously.[12] Quantitative analysis was performed using the CFX96 Real-Time System (BioRad) with Ssoadvanced SYBR Green SuperMix (BioRad). The sequences of the primers used were as follows:

miR-1246 forward: 5′-GCTTGGCTAGCTGCCTTAACA-3′
miR-1246 reverse: 5′-GGATCTGCAGGCACTAACTTGTAG-3′.
miR-302a forward: 5′-GGGTAAAAGGCAGGGACTTC-3′,
miR-302a reverse: 5′-CAGACCCACCCAGGATCATA-3′.
miR-4448 forward:5′-TATTACCTGCGTCCGAGGAG-3′
miR-4448 reverse:5′-CTCGTGCTCTATGGTGTTGC-3′

The fraction of immunoprecipitated DNA was calculated as follows: (DNA immunoprecipitated with EZH2 or p53 antibody—negative control with IgG)/(input DNA—negative control with IgG). Experiments were carried out in triplicate.

Western blotting

Protein extracts were separated by SDS/polyacrylamide gel electrophoresis and transferred to nitrocellulose membranes, and the membranes were hybridized with the antibodies described above. β-Actin was used as an internal control.

Apoptosis assay

AGS and HepG2 cells were cultured in media supplemented with 10% FBS and treated with 1 μM SAHA and 5 μM DZNep for 72 h. Apoptosis assay was

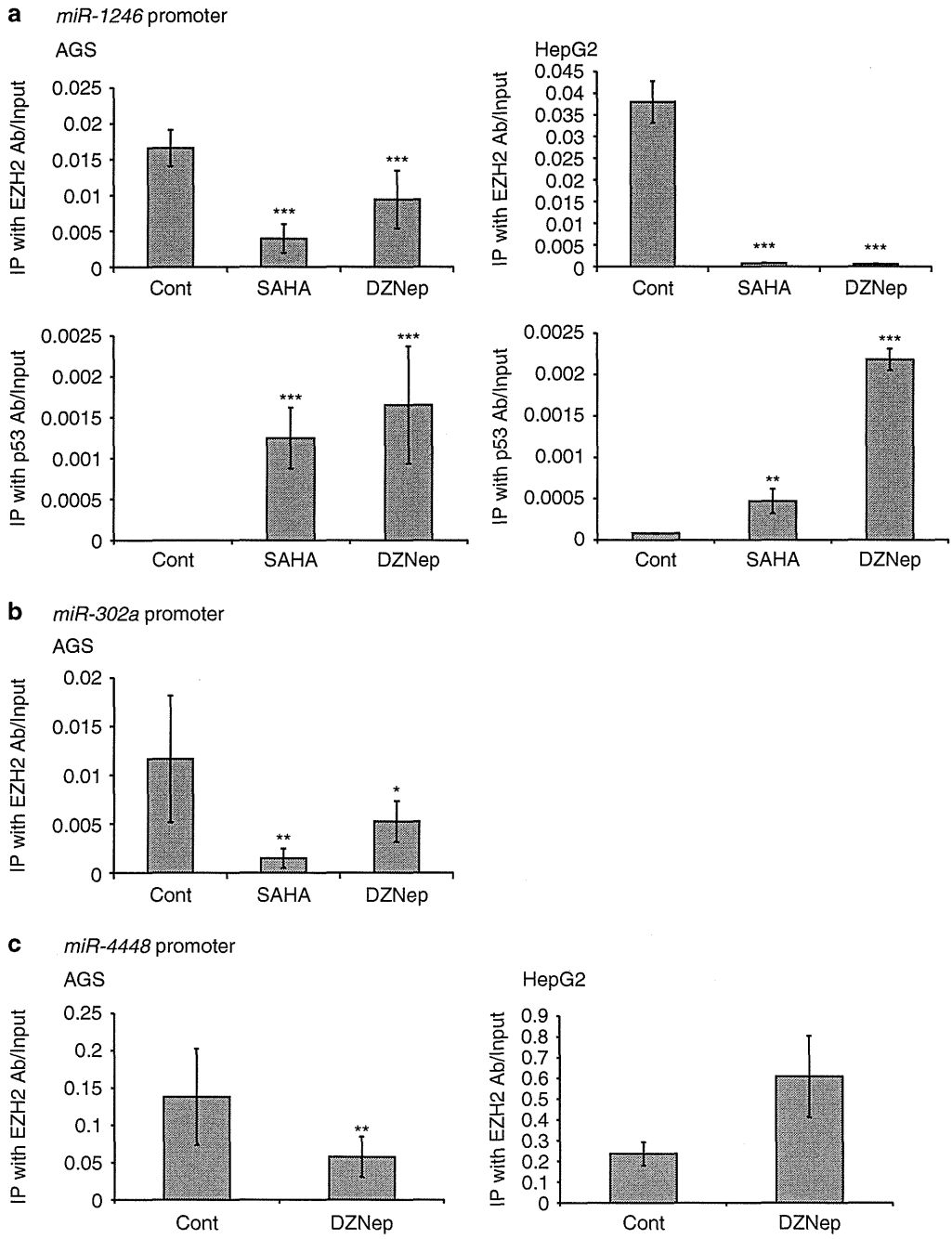

Figure 6. ChIP assays of binding of anti-EZH2 and -p53 antibodies to the promoter regions of *miR-1246, miR-302a and miR-4448.* (**a**) ChIP assay to determine binding of antibodies against EZH2 and p53 to the promoter region of *miR-1246* in AGS and HepG2 cells treated with SAHA and DZNep. $^{**}P<0.01$, $^{***}P<0.001$. (**b**) ChIP assay to determine binding of anti-EZH2 antibody to the promoter region of *miR-302a* in AGS cells treated with SAHA and DZNep. $^{*}P<0.05$, $^{**}P<0.01$. (**c**) ChIP assay to determine binding of anti-EZH2 antibody to the putative promoter region of *miR-4448* in AGS and HepG2 cells treated with DZNep. $^{**}P<0.01$.

performed using an Annexin V-FITC Apoptosis Detection Kit (Bio Vision, Milpitas, CA, USA). Flow cytometry analysis was performed using BD FACSDiva (BD Bioscience). The data are indicated as mean ± s.d. for three independent experiments.

Cell cycle assay

AGS and HepG2 cells were cultured in media supplemented with 10% FBS and treated with 1 μM SAHA and 5 μM DZNep for 72 h. Cells were harvested by trypsinization, washed with PBS, and then fixed in 70% ice-cold ethanol overnight at 4 °C. They were then washed with PBS and treated with RNase A (1 mg/ml) at 37 °C for 60 min and incubated with propidium iodide (50 μg/ml) for 30 min at room temperature. After incubation, flow cytometry analysis was performed using a BD FACSDiva (BD Bioscience).

Sphere-forming assay

For sphere-forming assay, we used ReproFF2 medium (Repro cell, Kanagawa, Japan), which is a new feeder-free culture medium for human ES/iPS cells. We also used the Ultra-low attachment surface (Corning, Corning, NY, USA), which is coated with a hydrogel layer and prevents attachment of cancer cells growing in an anchorage-dependent manner.[40] AGS and HepG2 cells were cultured in serum-free ReproFF2 medium containing 5 ng/ml bFGF with 5 μM DZNep or 1 μM SAHA in a 96-well plate